An Acad Bras Cienc (2025) 97(Suppl. 2): e20241163 DOI 10.1590/0001-3765202420241163
Anais da Academia Brasileira de Ciências | *Annals of the Brazilian Academy of Sciences*
Printed ISSN 0001-3765 I Online ISSN 1678-2690
www.scielo.br/aabc | www.fb.com/aabcjournal

BIOMEDICAL SCIENCES

New Tacrine Dimers Alleviate the Intracellular Amyloid-β-induced Cognitive Disturbance and Oxidative Stress in Mice

ANA ELISA GONÇALVES, OTTO SPIGARIOL, LUÍSA M. DA SILVA, YURI F. REGO, CLARA HERRERA-AROZAMENA, MARÍA ISABEL RODRÍGUEZ-FRANCO, ÂNGELO DE FÁTIMA, THIAGO HENRIQUE DORING, LUCAS AUGUSTO ARAUJO, MARIA LÍGIA R. MACEDO, SUMBAL SABA, JAMAL RAFIQUE, ALDO S. OLIVEIRA & MÁRCIA MARIA DE SOUZA

Abstract: This study aimed to investigate *in vivo* and *ex-vivo* the effects of tacrine dimers (TD1, TD2, TD3 and TD4) in mice with Alzheimer's disease (AD) induced by amyloid peptide (Aβ42) and, respectively, evaluated in behavioral tests of cognition, oxidative stress and neuroinflammation. All dimers reduced the cognitive deficit caused by Aβ42, oxidative stress and neuroinflammation, especially the compound TD4. By ADMET analysis (SwissADME and pkCSM 2.10 platforms), TD4 exhibited favorable pharmacokinetic properties with the control drug. The results suggest a therapeutic potential for AD for these compounds, given their distinct cognitive and neuroprotective effects in AD models induced by Aβ42.

Key words: Tacrine Dimers, Amyloid-β (Aβ42), Cognitive Disturbance, Oxidative Stress, Neuroprotection.

INTRODUCTION

Unquestionably, Alzheimer's disease (AD) is the main cause of dementia worldwide, posing a significant public health concern for the aged in the twenty-first century. Alzheimer's disease is defined by a steady deterioration in cognitive functions, which is accompanied by behavioral symptoms. In the preclinical phase of AD, known as the cellular phase, interactions among neurons, microglia, and astroglia contribute to the gradual progression of the disease before cognitive symptoms manifest. Neuroinflammation, vascular changes, aging, and glymphatic system dysfunction all contribute to the accumulation of amyloid β in this condition. Amyloid β promotes the spread of tau disease, resulting in necroptosis markers in neurons with granulovacuolar degeneration (Scheltens et al. 2016). Oxidative stress is associated with AD progression by promoting Aβ deposition, tau hyperphosphorylation, and the subsequent loss of synapses and neurons (Cioffi et al. 2021).

The G8's most economically developed countries announced that dementia had become a global priority, requesting, and emphasizing the availability of a satisfactory cure or medication by 2025 (Scheltens et al. 2016). Currently, there are few medications available for the treatment of Alzheimer's disease that merely treat symptoms and do not modify the disease's progression (Breijyeh & Karaman 2020). These therapies include acetylcholinesterase (AChEI) inhibitors donepezil, galantamine, rivastigmine, and an NMDA receptor antagonist memantine

(Khan et al. 2020). Overall, the efficacy of the three ChE-Is on the market is similar, and the advantage of administering these compounds is minimal and may not be clinically meaningful. Efforts in medicinal chemistry and drug delivery research have aimed to enhance the pharmacological efficacy of ChE-Is while minimizing gastrointestinal side effects. Despite their limited efficacy and the need for more effective techniques, ChE-Is remain a valuable pharmacotherapeutic resource for the treatment of Alzheimer's disease (Marucci et al. 2021).

Tacrine (TAC) was the first anticholinesterase medication licensed by the FDA for the treatment of Alzheimer's disease, but it was withdrawn from the market due to hepatotoxicity (Wu et al. 2017). Several molecular modification procedures have been used to improve its pharmacological profile, including dimerization of TAC with various linkers (de Aquino et al. 2013). In contrast to standard therapeutics, the creation of tacrine dimers capable of binding to various pharmacological targets is currently of significant interest in AD, since it can decrease disease progression beyond symptoms (Hamulakova et al. 2021, Mohamed et al 2016, Roldan-Pena et al. 2017). In addiction, multifunctional compounds like tacrine dimers offer the advantage of targeting multiple pathological pathways simultaneously, potentially yielding synergistic effects that address both cognitive deficits and neuroinflammation in AD models.

As part of our larger research interest in the synthesis and biological evaluation of heterocyclic compounds (Botteselle et al. 2021, Burker et al. 2023, dos Santo et al. 2021, 2022, Fermiano et al. 2024, Franco et al. 2021, Frizon et al. 2020, Moraes et al. 2023, Pedroso et al. 2023, Rafique et al. 2020, Scheide et al. 2020, Veloso et al. 2021), this study explores four tacrine dimer derivatives (TD1, TD2, TD3, and TD4) to evaluate their neuroprotective potential in an AD mouse model and their biological features. Previously, fifteen novel tacrine dimers were produced, which demonstrated mixed inhibition against cholinesterase enzymes *in vitro* (de Aquino et al. 2013). This report evaluates the neuropharmacological effects of four promising new tacrine dimers (Figure 1) in mice with AD induced by the Aβ42 peptide. This study centers on assessing the cognitive, oxidative, and neuroinflammatory outcomes of tacrine dimers in AD models, highlighting these compounds as promising multifaceted therapeutic candidates for AD.

MATERIALS AND METHODS

Tacrine dimers

All four tacrine dimer molecules (TD1, TD2, TD3, and TD4), were synthesized previously in our laboratories (de Aquino et al. 2013).

Ethics statement

All animal-related procedures adhered to international norms and ethical animal welfare recommendations. The Institutional Ethics Committee on the Use of Animals at UNIVALI (Itajaí, SC, Brazil) authorized this study's experimental procedures by approval certificate 11/16.

Animals

The tests used Swiss male mice that were 10 to 12 weeks old and weighed 25 to 35 grams, obtained from UNIVALI's central laboratory. The housing conditions were maintained to maintain an ambient temperature of 22 ± 2 °C, humidity at 60%, a 12-hour light/dark cycle, and constant access to food and water. Following the completion of the behavioral investigations, euthanasia was performed, and the encephalon was removed for biochemical examination.

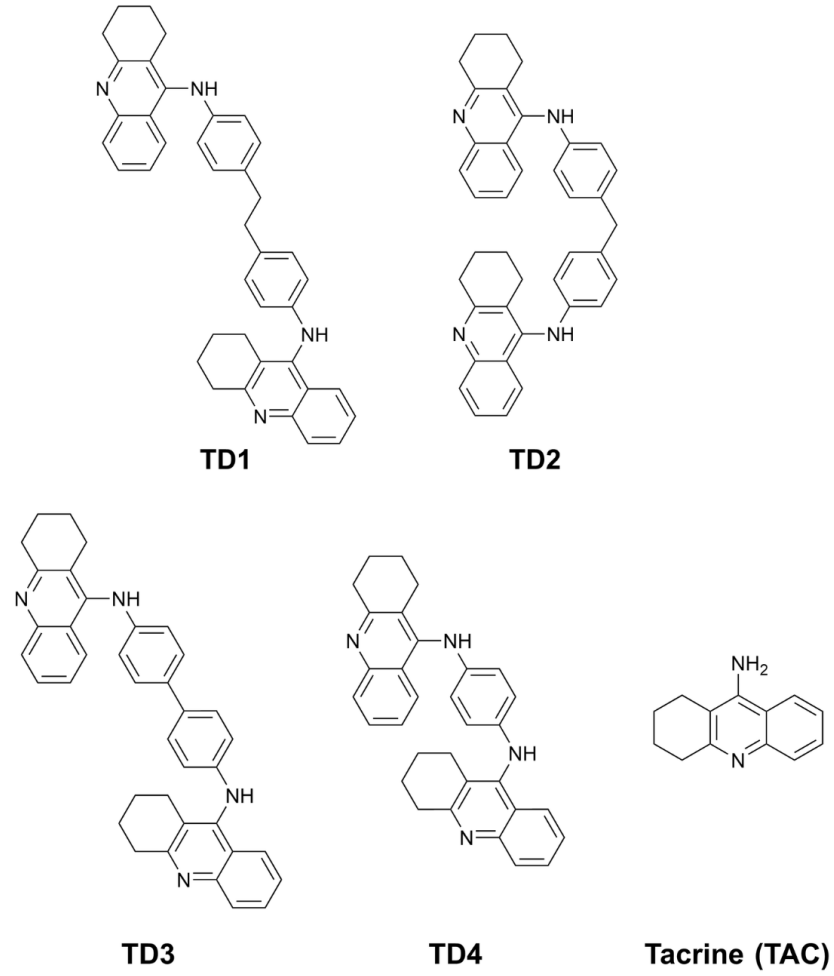

Figure 1. Tacrine dimers TD1, TD2, TD3 and TD4.

Groups and treatments

In the pharmacological component of this study, the mice were divided into eight groups with eight mice each, as follows:

- Group I, Naïve: This group did not receive therapy or intracerebroventricular (i.c.v) injection, establishing behavioral baselines to compare with rats exposed to β-amyloid peptide.
- Group II, Sham: This group received the vehicle (saline, 3 µL, i.c.v) used to dissolve the β-amyloid peptide, to ensure that the i.c.v. administration does not produce hippocampus injury, which could alter behavioral and biochemical outcomes.
- Group III, Control: This group was given an intravenous injection of Aβ42 peptide (3 µL, 400 pmol/animal) to induce Alzheimer's disease. They were given the vehicle used to solubilize the dimers (2% DMSO in distilled water) orally for 15 days.
- Group IV, Positive Control (TAC): This group was treated identically to Group III but received oral tacrine (50 µmol/kg, dissolved in water) for 15 days. Prior investigations have shown that oral TAC at 10 mg/kg (equal to 50 µmol/kg) improves

behavioral outcomes in mice (Baral et al. 2015).

- Groups V–VIII, Tacrine Dimers (TD1, TD2, TD3, TD4): Each group received both an intravenous injection of Aβ42 peptide (3 µl, 400 pmol/animal) and a 15-day oral treatment with the tacrine dimer compounds (TD1, TD2, TD3, TD4). The oral treatments were given at a molar dose equivalent to the normal TAC dose (50 µmol/kg), dissolved in 2% DMSO in distilled water.

Induction of Alzheimer's through administration of intracerebroventricular β-amyloid peptide (Aβ42)

According to one-way ANOVA, the intracerebroventricular (i.c.v.) administration of the β-amyloid peptide (Aβ42) reduced the locomotor activity. For this administration, mice were suitably anesthetized with a combination of xylazine and ketamine (10 and 100 mg/kg, respectively, i.p.). After assessing postural reflexes, a local anesthetic with a vasoconstrictor (2% xylestesin, s.c.) was administered to the upper head area. This was followed by an incision to remove the skin and reveal the skull cap. After surgery, the animals were placed in a heated, lit recovery box (40W) to prevent anesthesia-induced hypothermia until they recovered completely. The following day, 3 µL of Aβ42 (400 pmol/mouse) was given following the manufacturer's instructions (Amoah et al. 2015, Cazarin et al. 2021, Prediger et al. 2007).

Behavioral evaluation of animals

The sequence of conducting the behavioral tests can be visualized in Figure S1.

Open Field Test (OFT)

The Open Field Test (OFT) was used to determine whether the chemicals altered the animals' motor systems, which could change the results of their behavioral performance in studies. This test used a wooden box of 40 x 60 x 50 cm, as previously described (Gonçalves et al. 2012). The box's flooring was divided into nine equal quadrants. Animals were placed in a box 60 minutes after receiving the β-amyloid peptide intravenously seven days later. We followed and documented their travels across the quadrants for 6 minutes, counting instances of exploratory behaviors such as rearing, in which the animal stands on its hind legs to explore its surroundings. Observations of decreased locomotor and exploratory activity during this test suggest depressed effects, which may alter the animals' motor systems (Gonçalves et al. 2012). Following the initial observations, the animals were given more than 15 minutes to explore the box freely, ensuring proper habituation before moving on to the next trials.

Novel Object Recognition Test (NOR)

The process followed the methodology established by Izquierdo et al. (1998) and was later adopted into our studies (Gonçalves et al. 2021). On the seventh day after i.c.v. administration of the β-amyloid peptide, the animals were placed in an open field with no objects for a 15-minute acclimation period. The next day, the same animals were presented to the apparatus again, but this time with object A, for a 10-minute training session. On the ninth day, the animals were subjected to another 10-minute exposure to the device with two objects: the familiar object A and a new object B. A recognition index (RI) greater than 0.5, showing that B was investigated more than A, was considered evidence of satisfactory memory recognition.

Inhibitory Avoidance Test (IA)

The animals underwent an inhibitory avoidance test based on the protocol outlined by (Izquierdo et al. 2016), with specific modifications (Gonçalves et al. 2021). Each animal was gently positioned on a platform measuring 2.5 cm in height, 7.0 cm in depth, and 25.0 cm in width, on the left side of an apparatus measuring 50 x 25 x 25 cm. The apparatus floor consisted of parallel stainless-steel bars, each with a diameter of 0.1 cm and spaced 1 cm apart. A 15W lamp illuminated the apparatus, and the surrounding room remained dark. During the training session, the time taken for the animal to place all four legs onto the grid was recorded as the descent latency. Subsequently, upon full contact with the grid, the animal's legs were immediately subjected to a mild electrical shock of 0.4 mA for 2.0 seconds.

In the subsequent test session, which took place 24 hours after the training session, the procedure mirrored that of the training session, except for the omission of the electrical shock. The descent latency was again recorded, with a maximum observation period of 180 seconds.

Morris Water Maze (MWM)

For this experiment, we employed an aquatic maze like the one detailed by Morris et al. (1982). The aquatic maze comprised a circular polyethylene tank, measuring 100 cm in diameter and 50 cm in height, filled with water maintained at a temperature of 25±1 °C. The maze was partitioned into four imaginary quadrants. Positioned 1.5 cm below the water surface in the center of one quadrant was a circular platform measuring 12 cm in diameter and 25 cm in height, which served as the target location for the animals to locate. Visual cues were affixed to the walls to aid spatial navigation.

A video camera was mounted above the water maze to record the experiment for subsequent analysis using ANY-Maze software (Stoelting Co.). Training commenced on the 10th day post i.c.v. administration of the β-amyloid peptide and spanned five consecutive days. Each daily training session involved placing the animal in the center of a quadrant, facing away from the maze's center, and allowing it to swim for a maximum of 60 seconds to locate the platform. When the animal arrived at the platform, it remained in place for 15 seconds; if unsuccessful, it was physically placed on the platform and permitted to stay for 30 seconds. After each session, the animals returned to their separate housing boxes to prepare for the training on the next day.

Escape latency, the time each animal took to locate the platform during each attempt, was recorded via image capture for subsequent analysis. It is anticipated that a reduction in escape latency over successive trials indicates spatial learning.

On the sixth day, a Probe trial was conducted, during which the platform was removed from the maze, and the animals were given 60 seconds of unrestricted swimming. The time spent in each quadrant during this trial was recorded for analysis. The accuracy of spatial learning was evaluated based on the time spent in the quadrant where the platform had been located during the training sessions. This analysis indicates the animal's utilization of spatial orientation strategies based on environmental cues (Barnhart et al. 2015).

Prediction of the brain penetration

The prediction of brain penetration was assessed using a parallel artificial membrane permeation assay for the blood-brain barrier (PAMPA-BBB), following established protocols (Herrera-Arozamena et al. 2020a, b, 2022, Valencia et al. 2018). Pipetting was conducted using a semi-automatic pipettor (CyBi®-SELMA), and UV readings were obtained using

a microplate spectrophotometer (Multiskan Spectrum, Thermo Electron Co.). Commercial drugs, phosphate-buffered saline solution at pH 7.4 (PBS), and dodecane were procured from Sigma-Aldrich, Acros, and Fluka. Millex filter units with PVDF membranes (diameter 25 mm, pore size 0.45 *μm*) were sourced from Millipore, while porcine brain lipid (PBL) was obtained from Avanti Polar Lipids.

The donor microplate used was a 96-well filter plate with PVDF membranes (pore size 0.45 *μm*), and the acceptor microplate was a 96-well plate with indented wells, both from Millipore. The acceptor microplate was filled with 200 *μL* of PBS: ethanol (70:30), while the filter surface of the donor microplate was coated with 5 *μL* of porcine brain lipid (PBL) in dodecane (20 mg/mL).

Compounds, dissolved in PBS: ethanol (70:30) at a concentration of 100 *μg*/mL, were filtered through Millex filters and added to the donor wells (200 *μL* each). The donor filter plate was then carefully placed onto the acceptor plate to create a sandwich configuration, which remained undisturbed for 120 minutes at 25 °C.

After the incubation period, the donor plate was removed and the concentration of chemicals in the acceptor wells was measured using UV-visible spectroscopy. Each sample was evaluated at five wavelengths in four wells, and the experiment was performed in at least three separate runs. The results are shown as means ± standard deviation. In addition, each experiment contained 11 quality control standards with known BBB permeability to confirm and normalize the data set.

Biochemical analysis

Preparation of the samples for evaluation of the cerebral antioxidant system

After completing the behavioral tests, the animals were euthanized via guillotine, and their brains were swiftly removed. The hippocampus was dissected, weighed, and homogenized in 200 mM potassium phosphate buffer (pH 6.5) at a ratio of six times the volume relative to the weight of each tissue.

The resulting homogenate was promptly utilized for quantifying the levels of reduced glutathione (GSH) and lipid hydroperoxides (LOOH). Subsequently, the homogenate was centrifuged for 20 minutes at 11,000 rpm at 4 °C using a microcentrifuge. The supernatant was utilized to measure the activity of superoxide dismutase (SOD), while the precipitate was used to determine the activity of myeloperoxidase (MPO).

All procedures to obtain homogenates and subsequent biochemical assays were conducted at 4°C to maintain sample integrity and prevent degradation.

Quantification of reduced glutathione (GSH) levels

The GSH levels in the brain and hippocampus were measured using the method reported by Sedlak & Lindsay (1968). In each tube, 50 µL of the homogenate was mixed with 40 µL of 12% trichloroacetic acid. The mixture was centrifuged at 4000 rpm for 15 minutes at 4°C.

Next, transfer 20 µL of the supernatant to a 96-well plate. Add 280 µL of 0.4M TRIS buffer (pH 8.9) and 5 µL of a 3.96 mg/mL solution of 5,5'-dithiobis-2-nitrobenzoic acid in methanol. After 15 minutes of incubation, spectrophotometric values were taken at 405 nm. Individual sample results were then interpolated using a standard curve of GSH ranging from 0.05 to 0.21 µg and expressed as µg GSH per gram of tissue.

Determination of superoxide dismutase (SOD) activity

The SOD activity was measured by Marklund & Marklund (1974). In each tube, 442.5 µL of TRIS HCl-EDTA buffer (pH 8.5) and 20 µL of sample supernatant were added. The mixture was combined with 25 µL of 1 mM pyrogallol. The sample was incubated at 25 °C for 20 minutes. After stopping the reaction with 12.5 µL of 1N HCl, the tubes were centrifuged at 14,000 rpm for 4 minutes. The supernatant (300 µL) was transferred to a 96-well microplate and measured at 440 nm using a spectrophotometer. The SOD activity was measured and represented as U/mg protein.

Determination of lipid hydroperoxides (LOOH)

The LOOH measurement in the cortex and hippocampus was performed using the methods reported by Jiang et al. (1992). In each microcentrifuge tube, 10 µL of methanol and 100 µL of homogenate were mixed. The tubes were then centrifuged at 11,000 rpm for 20 minutes at 4°C. Transfer 30 µL of the supernatant to a 96-well plate, then add 140 µL of the reaction medium (100 mM orange Xylenol, 250 mM Iron II, and 4 mM butylated solubilized in methanol). The mixture was then incubated for 30 minutes at 25°C in the dark. After incubation, the absorbance was measured at 560 nm with a spectrophotometer.

Quantification of myeloperoxidase (MPO) activity

The resulting homogenate was centrifuged at 10,000 rpm for 20 minutes. The precipitate was resuspended in 500 µL of 80 mM potassium phosphate buffer with 0.5% hexadecyltrimethylammonium. After homogenization, the samples were centrifuged at 11,000 rpm for 20 minutes at 4°C in a chilled microcentrifuge. Duplicate aliquots of 30 µL of each sample's supernatant were added to 200 µL of a reaction solution consisting of 100 µL of 80 mM phosphate buffer, 85 µL of 22 mM phosphate buffer, and 15 µL of 0.017% H2O2 in a 96-well plate. To start the reaction, 20 µL of tetramethylbenzidine was added to each well. After 3 minutes of incubation at 37°C, each well was treated with 30 µL of 1.46 M sodium acetate (pH 3.0) to end the reaction. The absorbance was measured at 620 nm with a spectrophotometer. The findings were presented as milli optical density units (mOD) per milligram of protein.

Protein Dosage

To calculate SOD and MPO activity, protein concentrations were determined using the Bradford assay, with bovine serum albumin as the standard (range from 1.0 to 0.025 µg/µL) (Bradford 1976). In a 96-well plate, combine 5 µL of the sample supernatant with 200 µL of Bradford reagent. The plate was then examined in a spectrophotometer at 560 nm.

Statistical analysis

The collected results were subjected to analysis of variance (ANOVA) for statistical purposes. When applicable, we used GraphPad Prism 8® software to perform Tukey's multiple post hoc comparison test. Results are reported as means ± standard deviation (SD), with statistical significance as $p<0.05$.

Computational Studies

Molecular Docking

For the molecular docking, the Hermes GOLD software (Genetic Optimization for Ligand Docking; version 1.10.5) was employed, following the methodology described by Verdonk et al. (2005). This software utilizes a genetic-type algorithm for ligand-receptor interaction.

Protein preparation was conducted using the APBS Biomolecular tool at pH 8.0 (Jurrus et al. 2018). ChemSketch 2021.1.1 software was used for the dimers design, in which the SMILES codes were created to generate the three-dimensional structure in Avogadro 1.2.0 (Hanwell et al. 2012). In Avogadro 1.2.0, a pre-optimization was performed using the Ghemical force field, until $\Delta E < 10^{-3}$ kJ/mol. The configuration of the ligands was performed in MarvinSketch 22.11 (Csizmadia 1999), using the microspecies/pKa distribution tool and setting the physiological pH to 8.0.

The human acetylcholinesterase receptor (PDB 4M0E) (Cheung et al. 2013) was handled as rigid, with flexibility allowing for rotatable bonds in the ligands, which were treated as fully flexible. Only chain A of both the receptor and the ligands was employed in the analysis. Crystallographic water molecules were removed, and the binding site was defined as encompassing all receptor atoms within a 6 Å radius of the reference crystallographic inhibitor. The top-scoring conformations were chosen for further analysis, with all other settings kept at their default values.

Quantum studies

Pre-optimization was conducted using Avogadro (version 1.2.0) (Hanwell et al. 2012) with the Chemical Force Field until the energy difference was less than 1×10^{-3} kJ/mol. Density functional theory (DFT) calculations were performed to estimate energy values in the vacuum phase. The highest occupied molecular orbital (HOMO) and lowest unoccupied molecular orbital (LUMO), as well as the energy gap (LUMO-HOMO), were computed using ORCA 5.0.2 (Neese 2012) with the B3LYP (Lee et al. 1988) functional and def2-TZVPP (Weigend & Ahlrichs 2005) basis sets. Molecular orbitals were generated using Chemcraft 1.8 (Zhurko & Zhurko 2005).

ADMET profiles

The ADMET analyses for the compounds were conducted using SwissADME (SwissADME tool) and pkSCM 2.10.2 (pkSCM tool). The SwissADME tool was employed to predict the pharmacokinetic properties, such as water solubility, intestinal absorption, Caco-2 permeability, and skin permeability, as well as to assess the potential of the compounds as P-glycoprotein (P-gp) substrates and inhibitors, and their interactions with various cytochrome P450 enzymes. Additionally, pkSCM 2.10.2 was used to calculate parameters related to drug absorption, distribution, metabolism, and excretion, providing insights into the compounds' overall pharmacokinetic profiles.

RESULTS

Evaluation of the effects of compounds on the mice's behavioral

Effect of treatments on locomotor activity.

One-way ANOVA established a significant decrease in locomotor activity (number of crossings) of animals treated with TAC and TD4 compared to the control group ($F_{7.56} = 3.233$, $p < 0.01$), as well as the group treated with TD4 had a significant reduction (Table SI). Furthermore, this significant reduction in locomotor activity is not observed when compared to the naïve or sham group. No notable differences were established in the number of creations between the groups ($F_{7.56} = 1.640$, $p = 0.1434$).

Effect of treatments on recognition memory through the Novel Object Recognition test.

In the test that evaluates recognition memory, the animals of the control group, which received only Aβ42, presented cognitive impairment compared to the Naïve group ($F_{7.56} = 8.144$, $p < 0.001$, Figure 2). This cognitive impairment

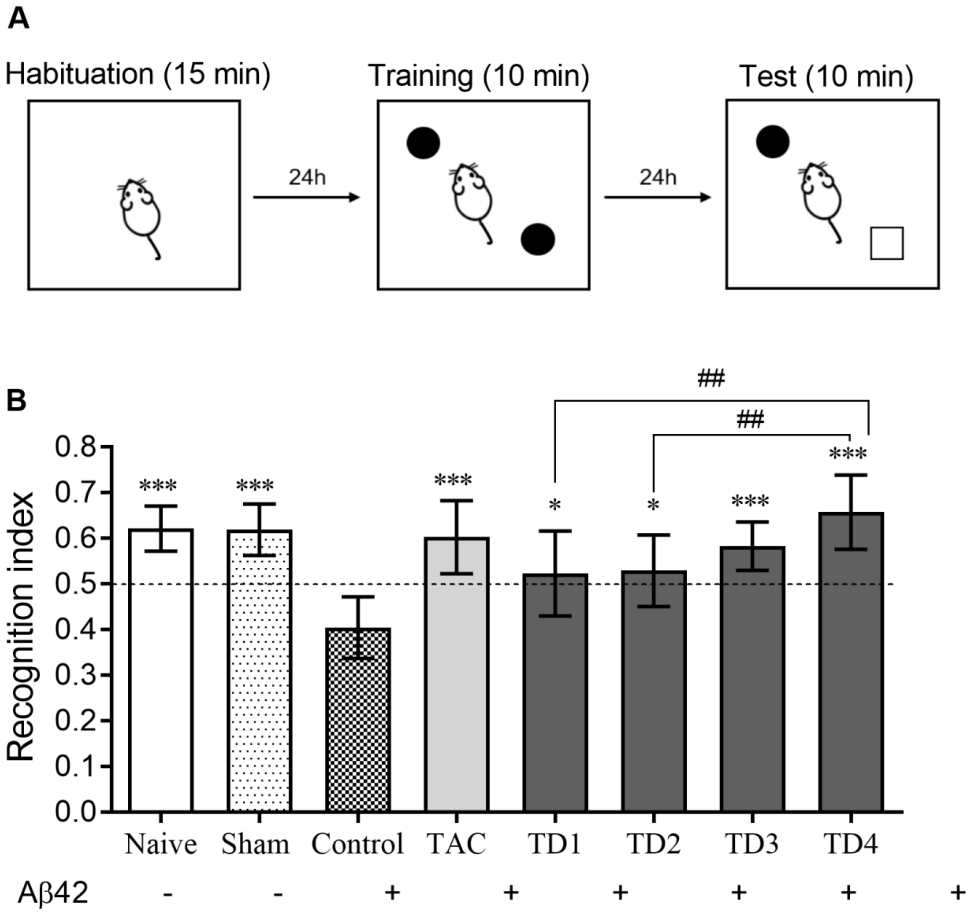

Figure 2. Panel a: schematic representation of the experimental protocol. Panel b: Means ± SD of recognition index of familiar object of mice submitted to the Novel Object Recognition test, calculated by dividing the amount of exploration of the novel object by the total amount of object exploration. n = 8 per group. One-way ANOVA, Tukey's post hoc test: ** p < 0.01 and *** p < 0.001 compared to the Control group (vehicle-treated mice).

caused by Aβ42 was reversed in the tacrine-treated group and the tacrine dimers-treated groups significantly increasing the recognition index of the familiar object compared to the control group. Interestingly, the TD4 compound was the one that best promoted an increase in the recognition index of the familiar object compared to the control group.

Evaluation of aversive memory of animals in the Inhibitory Avoidance test.

In the Inhibitory Avoidance test, the descent latency parameter was used to evaluate tacrine dimers' effects on the aversive memory of the animals. The results are shown in Figure 3. As expected, the i.c.v. administration of Aβ42 in mice resulted in a 56 % decline in cognitive function, as demonstrated by the decrease in latency of descent in the test session of the control group compared to normal animals (naïve) ($F_{7,56}$ = 16.75, p < 0.001). The treatment with TAC and the tacrine dimers reversed the cognitive impairment compared to the control group.

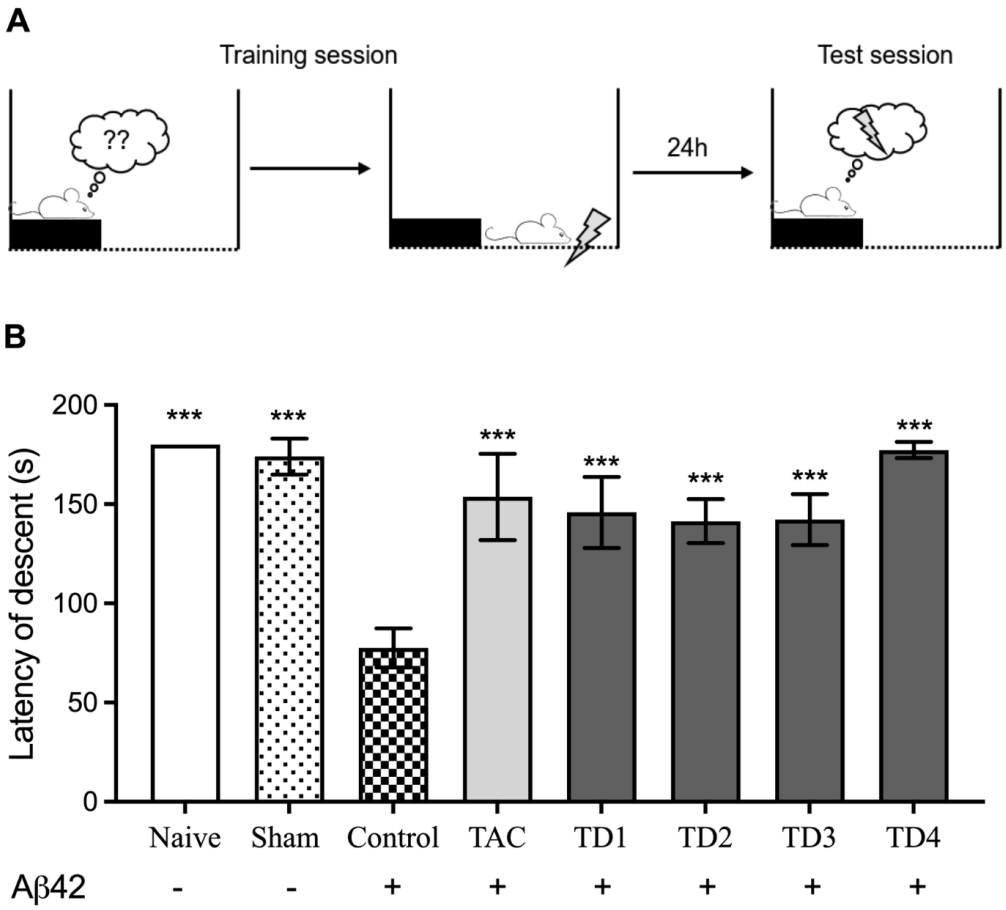

Figure 3. Panel a: schematic representation of the experimental protocol. Panel b: Mean ±SD of time spent on target quadrant (s) during the probe trail after 5 days of daily training. n = 8 per group. One-way ANOVA, Tukey's post hoc test: *** p < 0.001 compared to the Control group (vehicle-treated mice).

Evaluation of spatial memory of animals through the Morris Water Maze test.

Figure 4 shows the Probe trial results, which is how long each group remained in the target quadrant during the 60 seconds of the trial session after 5 days of daily training. Compared with the group of normal animals (Naïve), the control group remained for less time in the target quadrant ($F_{7,56}$ = 13.37, p < 0.001), suggesting a deficit in spatial cognition. The TAC group and tacrine-dimers group were significantly better than the control group (p < 0.001) and, again, the treatment of the animals with TD4 was the one that best promoted the improvement of the cognition of the animals, reversing the effects of the amyloid peptide.

Prediction of the CNS-Permeation.

Brain penetration was predicted using the in vitro PAMPA-BBB assay modified by a part of us for testing molecules with limited water solubility (Herrera-Arozamena et al. 2020a, b, 2022, Valencia et al. 2018). The compound permeability value (Pe) through a lipid extract of the porcine brain was determined using PBS: ethanol (70:30) as a solvent for 2h at room temperature, and results are gathered in Table SII. In the same assay, 11 commercial drugs of known CNS penetration were also tested, and their permeability

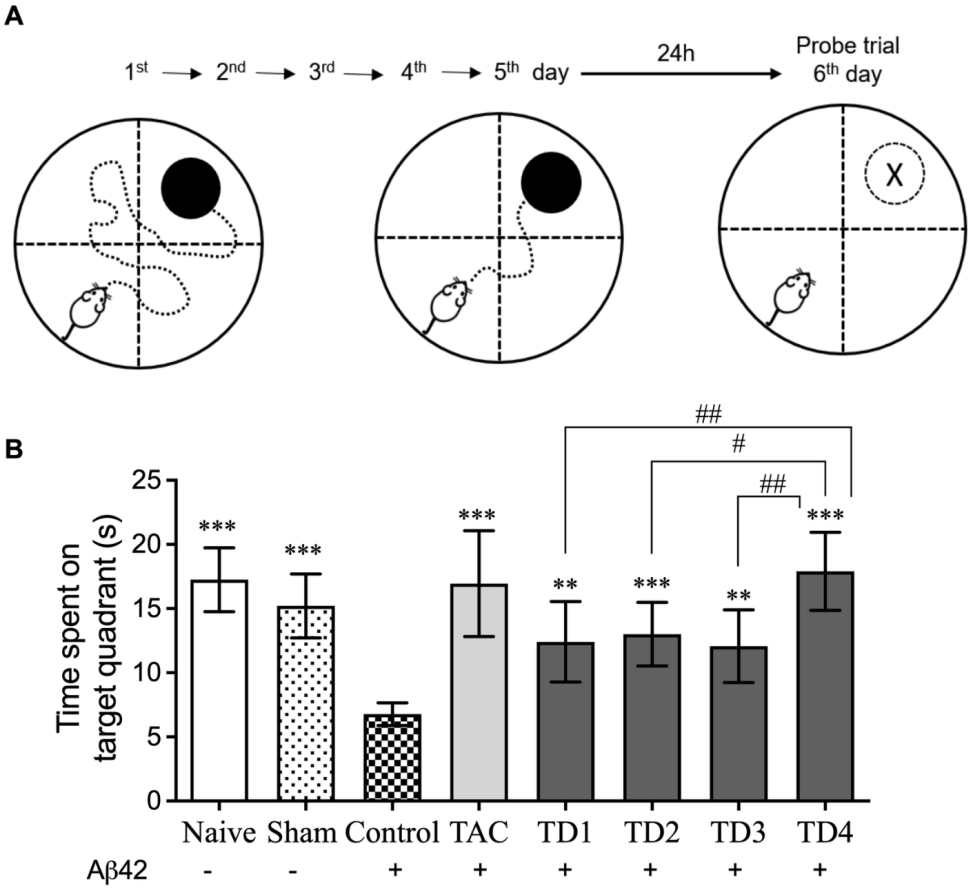

Figure 4. Panel a: schematic representation of the experimental protocol. Panel b: Latency of descent (s) of mice submitted in Inhibitory Avoidance test 24h after training. n = 8 per group. One-way ANOVA, Tukey's post hoc test: ** p < 0.01 and *** p < 0.001 compared to the Control group (vehicle-treated mice).

values were compared and normalized to the reported data. Tacrine and galantamine were also evaluated for comparative purposes. Compounds TD1, TD2, and TD3 were insoluble in the assay medium, therefore no data from these are shown. According to the patterns previously established in the bibliography (Di et al. 2003), compounds with Pe exceeding $4{\cdot}10^{-6}$ cm/s would be able to cross the blood-brain barrier, whereas those displaying Pe less than $2{\cdot}10^{-6}$ cm/s^{-} would not reach the CNS. Tested compounds (TD4, TAC, and GAL) showed permeability values above 4·10-6 cm/s in this in vitro BBB model (Table SII), it is expected they could enter the CNS by passive diffusion and interact with their biological targets.

Evaluation of the effects of compounds in the mice hippocampus.

Table SIII shows the results of the effects of treatments on the levels of GSH, LOOH, and activities of SOD, and MPO in the hippocampus of animals. The Control and TAC groups presented a significant decrease in the GSH levels compared to the Naïve group ($F_{7,56}$ = 32.6, p < 0.001), and treatments with tacrine dimers (TD1, TD2, TD3, and TD4) increased GSH levels compared to the TAC group. The results demonstrate that the hippocampus of the Control, TAC, and TD1 groups

had an increase in the SOD activity compared to the naïve group. The TD2, TD3, and TD4 treated groups showed a significant decrease in the SOD activity compared to the TAC group ($F_{7,56}$ = 33.74, p < 0.001).

Control, TAC, TD1, TD2, and TD3 groups increased the LOOH levels compared to the naïve group. In contrast, TD4 presented lower levels than TAC ($F_{7,56}$ = 33.4, p < 0.001). Aldo, the Control and TAC groups show increased MPO activity compared to the naïve group. While the tacrine dimers (TD1, TD2, TD3, and TD4) decreased MPO activity concerning the TAC group ($F_{7,56}$ = 12.8, p < 0.001).

DISCUSSION

With the increasing advances in modern medicine, human life expectancy increases every day, and for this reason, the prevalence of diseases whose risk factor is old age has also increased, including Alzheimer's disease (AD) (Lopez & Kuller 2019).

As previously reported (Cioffi et al. 2021, Breijyeh & Karaman 2020, Scheltens et al. 2016), AD is a neurodegenerative disease whose neurodegeneration process begins in the hippocampus (which plays an important role in recent memory functions) and expands throughout the CNS (Pluta et al. 2021). The expansion of the disease to extrahippocampal areas results in other dysfunctions, in addition to memory disorders, leading to symptoms strictly related to dementia, as well as neuropsychiatric manifestations, such as depression and anxiety (Martín-Sánchez et al. 2021, Pentkowski et al. 2021, Pluta et al. 2021). AD appears to be caused by genetics and specific protein dysfunctions related to TAU protein and amyloid precursor protein (APP), which result in the formation of histopathological findings characteristic of the disease: neurofibrillary tangles and amyloid plaques, as well as cytotoxicity, oxidative stress and neuroinflammation (Scheltens et al. 2016). It is not known which of the events listed above initiates the neurodegenerative process. Most drugs approved for the treatment of AD are acetylcholinesterase inhibitors (AChEIs), such as tacrine, rivastigmine, donepezil, and galantamine (Khan et al. 2020, Moss & Perez 2021). However, these medications have limited palliative therapy because they only improve memory deficits in the early stage of the disease but do not stop the neurodegenerative process (Kaushik et al. 2018, Marucci et al. 2021).

Because AD has a complicated etiology and complex pathophysiology, there are currently no medications that can treat all pathophysiological components of the disease. As a result, developing suitable treatments has proven difficult (Yu et al. 2015). The search for multifunctional compounds capable of interacting with diverse biological targets linked to the disease, known as Multi-Targeted Ligands (MTDLs), is a promising therapeutic method (Simoni et al. 2017, Waly et al. 2022). Hybridization of tacrine in the form of dimers, for example, produces MTDLs capable of operating as bivalent AChEIs while providing considerable neuroprotection against oxidative stress and neuroinflammation (Nepovimova et al. 2021, Qian et al. 2014, Spilovska et al. 2017, Balducci & Forloni 2014). Our laboratories synthesized and studied the dimers TD1, TD2, TD3 and TD4, which showed that these types of dimerization ligands modulate the electronic properties of the studied tacrine (TAC) dimers with an improvement in their cholinesterase inhibition activity (de Aquino et al. 2013), and this gave us led to continue *in vivo* studies with these compounds.

Central administration of the Aβ42 peptide in laboratory animals is a valuable model for studying AD and potential neuroprotective

therapies (Balducci & Forloni 2014). It is reported in the literature that this model imitates one of the initial stages of disease manifestations, the formation of amyloid plaques and its pathophysiological consequences with glial activation (Nakai et al. 2021). Compared to others, this animal model is considered one of the most specific for the study of AD, and the alteration or prevention of the effects resulting from the injection of the Aβ42 peptide into the brain of rodents, mainly cognitive deficits, is an important factor in the study of potential therapeutic targets for the disease (Esquerda-Canals et al. 2017). Our results corroborate and complement previous studies, which show that Aβ42 causes damage to different types of memory, decline in endogenous antioxidant functions, increased lipoperoxidation and neuroinflammation (Chang et al. 2014, Chen et al. 2015, Delgado-Peraza et al. 2021, Fu et al. 2014, Jiang et al. 2016, Mishra et al. 2013, Shen et al. 2016, Yu et al. 2015).

This study aimed to evaluate the impact of tacrine dimers on different types of memory in mice with Aβ42-induced AD. Memory disorders can occur in both neuropsychiatric and neurodegenerative diseases. In AD especially, the process of neurodegeneration can impair some types of memory, leaving others intact (Au et al. 2016, Shrestha & Klann 2016). Spatial memory impairments are reported in the early stages of AD, and spatial memory loss is linked to right hippocampal neurodegeneration (Parizkova et al. 2018). As the condition progresses, it becomes more difficult to consolidate new declarative memories, and those that have been preserved throughout the patient's life are gradually lost, causing the patient to lose their own identity. Therefore, animal memory tests are essential for the study of substances with anti-Alzheimer's potential.

In the present study, three different types of tests were used. The New Object Recognition Test (NOR) provides an experimental basis for investigating cognitive and neuropsychological processes in rats and mice. This recognition uses episodic declarative memory, subject to modifications and rapid loss (Lueptow 2017). We demonstrated that treatment with TAC and the dimers reversed the amnesic effect caused by Aβ42. Although episodic memory was quickly erased, retaining only episode-specific information, the animals preserved a statistically significant recognition rate after 24 hours of exposure.

Aversive memory deficits, whether procedural or declarative, also occur in AD (Fotuhi et al. 2020). Aversive memories are processed in the hippocampus, but there are important neural circuits in the amygdala (Chaaya et al. 2018, Terranova et al. 2022). This type of memory has been studied in different animals, whether vertebrates or invertebrates (Azambuja et al. 2018, Perathoner et al. 2016). In this study, we used an inhibitory avoidance (IA) test to evaluate the effects of compounds on aversive memory deficits induced by the Aβ42 peptide. The IA assesses memory related to the aversive stimulus, which involves fear conditioning mechanisms (Crystal 2016, Izquierdo & Medina 1997). As previously described, the Aβ42 peptide causes cognitive impairment assessed in IA (Cazarin et al. 2021, Shen et al. 2016), and studies show that AChEIs have positive effects reversing the deficits caused by the Aβ42 peptide (Gonçalves et al. 2021, Jafari et al. 2006).

The third memory test we used was Morris Water Maze (MWM). In rodents, maze tests such as the MWM are used to explore both working memory and reference memory, which are embedded in the context of spatial memories (Barnhart et al. 2015, Tian et al. 2019). After five days of consecutive daily training using

extra-maze distal cues, animals should be able to locate a submerged platform according to the methodology. In this study, the time spent measuring the target quadrant shows that the tested compounds have a promising therapeutic effect on this type of memory. The data presented reflect the beneficial effects of the treatment in terms of parameters such as the distance covered, swimming speed and the performance of the animals throughout the training days. Thus, together, our results demonstrated that animals subjected to the Alzheimer's model with Aβ42 treated with tacrine dimers and evaluated in different animal tests for different types of memory showed reversal of the cognitive deficits induced by Aβ42.

It has been demonstrated that the Aβ42 peptide causes intracellular oxidative stress by interacting with neuron lipid bilayers, releasing free radicals, and disrupting brain homeostasis (Sharma & Goyal 2020, Söllvander et al. 2016). This study found that mice treated with Aβ42 showed different results than normal animals (Naïve), supporting previous research on the peptide's effects on oxidative stress. GSH plays an important role in the reactive oxygen species (ROS) detoxification and in turn in the modulation of intracellular redox state (Raza et al. 2022). Several in vivo and in vitro investigations have demonstrated the protective role of GSH against various types of oxidative stress (Charisis et al. 2021). Aβ42 neurotoxicity in neurons and astrocytes may be related to GSH depletion, supporting the concept that AD pathogenesis is associated with GSH abnormalities. Additionally, the presence of this enzyme is neuroprotective and reduces oxidation induced by the peptide (Islam 2017, Raza et al. 2022). In this study, tacrine therapy did not affect the antioxidant defense process. However, tacrine dimers dramatically increased GSH levels in the presence of Aβ42 and lowered GSH in the hippocampus of mice that received Aβ42.

Another key antioxidant enzyme, SOD, catalyzes the conversion of superoxide radicals to hydrogen peroxide. There is considerable evidence linking SOD with AD (Hassanzadeh et al. 2015, Islam 2017, Mota et al. 2015, Persichilli et al. 2015, Zhang et al. 2015). In our trials, animals treated with Aβ42 had higher SOD activity than those treated with TD2, TD3, and TD4, which were identical to normal animals. The increased SOD can be explained by the high concentration of superoxide radicals, which necessitates increased enzymatic activity. Glutathione peroxidase (GPx) consumes more GSH to remove ROS as the conversion of superoxide anion increases. To better understand how tacrine dimers work, the antioxidant system will need to be evaluated further by dosing GPx and catalase.

The increase of free radicals causes oxidation of the lipid bilayer initiated by a self-perpetuating chain reaction, amplifying the initial oxidative event. In AD the lipoperoxidation of neurons is evident in all phases of the disease (Bradley-Whitman & Lovell 2015, Gaschler & Stockwell 2017). What we observed in our experiments is that the control group showed an increase in lipid hydroperoxides (LOOH), corroborating with the findings of Aguirre-Rueda et al. (2015), who demonstrated that the Aβ42 peptide decreases cell viability, and increases LOOH and apoptosis of neurons. Our results also showed increased levels of LOOH in TAC, TD1, TD2, and TD3 groups. However, the TD4 group showed levels of LOOH as low as normal animals (naïve). The mechanism by which only TD4 has been protected has not yet been elucidated, therefore further experiments must be performed to identify it.

To complement the investigation of the neuroprotective effect of the compounds under study, we evaluated the activity of MPO, which

is widely associated with inflammatory events, when released by migrating neutrophils, and in the brain by microglia (Gellhaar et al. 2017). Currently, MPO is related to neurodegenerative diseases and linked to the pathogenesis of inflammatory processes, oxidative stress and apoptosis (Fang et al. 2022, Ray & Katyal 2016). Furthermore, there is data in the literature demonstrating that there is co-localization of MPO with β-amyloid plaques around pyramidal granule neurons and the hippocampus in the brains of AD patients, indicating their possible contribution to the pathology of the disease (Gellhaar et al. 2017, Green et al. 2004). Our results showed that the Aβ42 peptide triggers neuroinflammation with increased MPO activity, and tacrine did not alter this process. Interestingly, the dimers under study, however, led to a decrease in MPO activity, which could indirectly reflect their possible anti-inflammatory activity. The mechanism is still uncertain, but there are indications that they may be acting directly on microglia, or this decrease may be a consequence of reduced oxidative stress, as happens with other representatives of this class of compounds (Zhang et al. 2021).

Interestingly, all compounds used in these studies showed anti-Alzheimer potential. However, compound TD4 was the most promising, with the highest efficacy compared to the other compounds in the series. In the previous cholinesterase inhibition in vitro study of the tacrine dimers, TD2 and TD3 were among the most potent inhibitors of human acetylcholinesterase, whereas TD4 was like TAC (Aquino et al. 2013). These trends in AChE inhibition did not translate to behavioral and biochemical improvements in this in vivo study, in which TD4 was significantly better than other dimers, shown more pronouncedly in the lower levels of LOOH in TD4-treated animals. Relating these differences among the series with structural differences of these compounds, the TD4 possesses the smallest distance among the tetrahydro acridine motifs and the least degree of conformational freedom. It is also possible to infer, that the mechanisms by which the studied compounds operate are more than simple cholinesterase inhibition. Another point of comparison between TAC and TD4 is the PAMPA assay for prediction of BBB permeation, in which TD4 presented almost double the Pe value of TAC, thus more lipophilic. That is possible due to increased symmetry in TD4 leading to a decrease in the dipole moment in the overall structure, provided by the 1,4-phenylene linker.

Computational studies

Molecular docking

To support the study of this article, molecular docking studies were performed to describe the mode of inhibition of dimers and the structure of human AChE (PDB ID 4M0E). Redocking with the Goldscore function was performed to validate the method, returning an RMSD of 0.336 Å as shown in Figure 5, confirming a high degree of alignment and low deviation. Tacrine was used as a reference standard for the studied dimers. In tacrine docking, the primary amine group forms a hydrogen bond with Asp74, but an unfavorable donor-donor interaction with Tyr124. Pi-alkyl interactions were observed for the side chains of Tyr337 and Phe338, and pi-pi stack interactions with Trp286 and Tyr341, according to Figure 6.

TD1 docking shows a hydrogen bond with Ser293 residue, and an unfavorable bump with Tyr124 and Tyr337, and this part of the structure may sterically interfere with the ligand-receptor docking. However, Tyr337 also has a pi-pi T-shaped interaction with the aromatic ring, as does Tyr341. Trp86 performs pi-pi stack

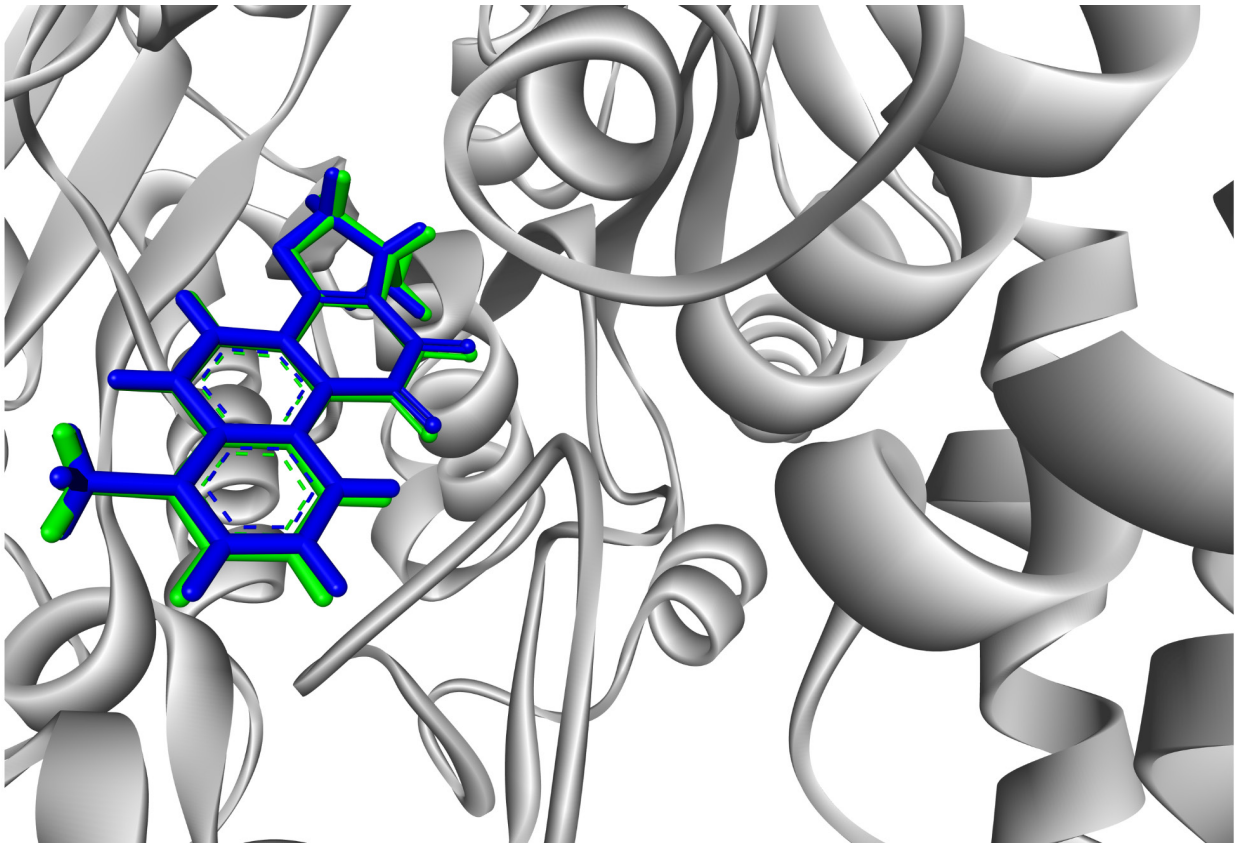

Figure 5. Redocking of the Dihydrotanshinone (1YL) ligand at the human acetylcholinesterase binding site (PDB ID 4M0E; peripheral anionic site). In green: is the best pose of the crystallized ligand generated by the GoldScore function; in blue: is crystallographic conformation. The figure was generated by the Biovia Discovery Studio Visualizer software (v21.1.0.20298, BIOVIA, San Diego, CA, USA).

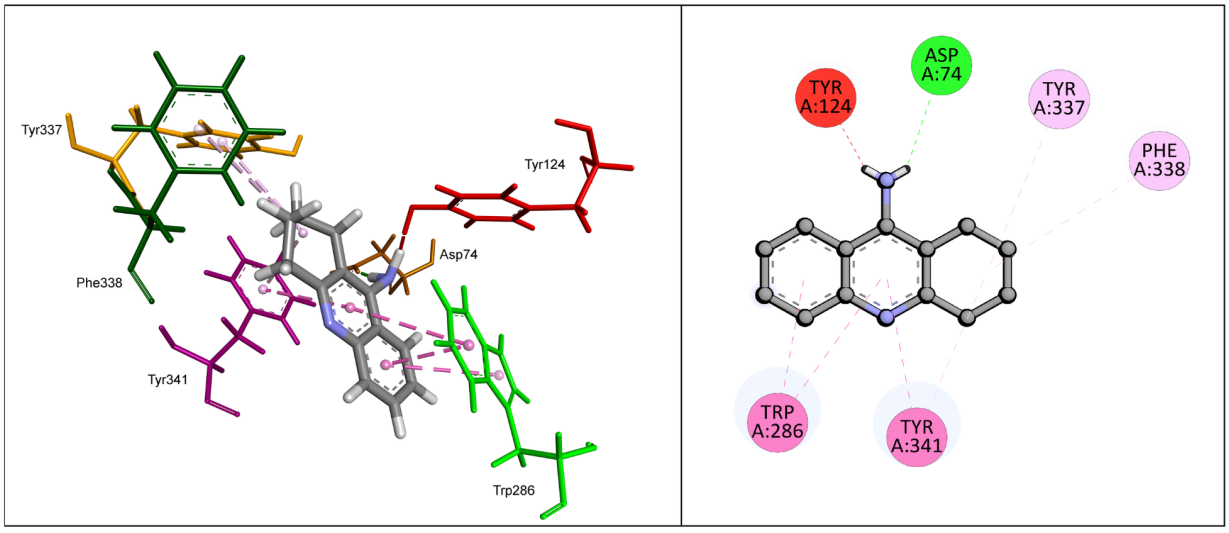

Figure 6. The 3D (left) and 2D (right) diagrams show the interactions of tacrine at the catalytic site of human acetylcholinesterase (PD ID 4M0E). The figure was generated by the Biovia Discovery Studio Visualizer software (v21.1.0.20298, BIOVIA, San Diego, CA, USA).

interaction with TD1, however, it also interacts via pi-sigma and pi-alkyl, as shown in to Figure 7.

For TD2, Tyr124 demonstrated a pi-lone pair interaction between the tacrine-derived aromatic heterocycle and the lone pair of the hydroxyl oxygen atom of the residue. Furthermore, Tyr 124 also makes pi-alkyl type interaction with the saturated cycle, as well as

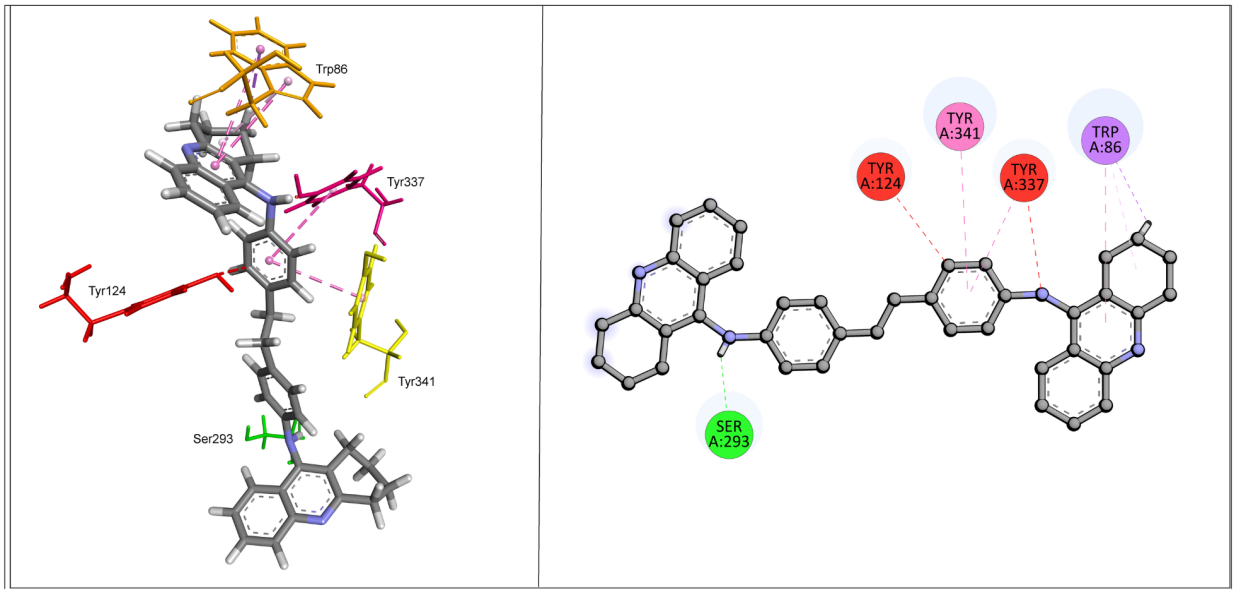

Figure 7. The 3D (left) and 2D (right) diagrams show the interactions of TD1 at the catalytic site of human acetylcholinesterase (PD ID 4M0E). The figure was generated by the Biovia Discovery Studio Visualizer software (v21.1.0.20298, BIOVIA, San Diego, CA, USA).

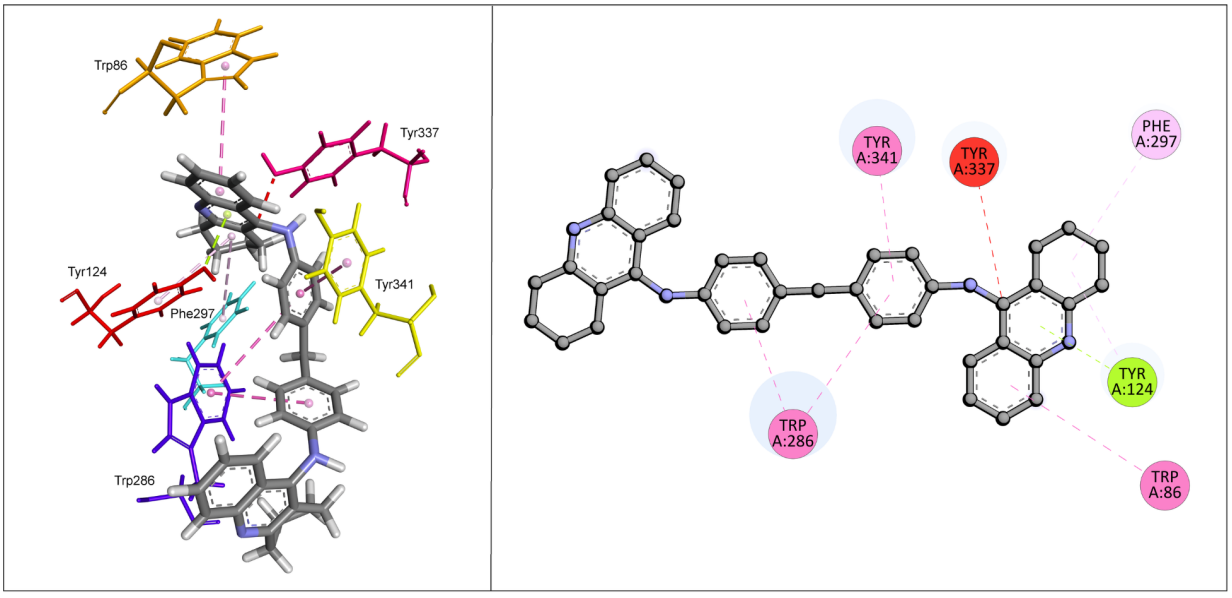

Figure 8. The 3D (left) and 2D (right) diagrams show the interactions of TD2 at the binding site of human acetylcholinesterase (PD ID 4M0E). The figure was generated by the Biovia Discovery Studio Visualizer software (v21.1.0.20298, BIOVIA, San Diego, CA, USA).

Phe297. A steric bump with the Tyr337 residue happens, in addition to pi-pi stack interactions with Tyr341 and pi-pi T-shaped interactions with Trp87. Trp287 has a pi-pi stack interaction with the top center ring and a pi-pi T-shaped interaction with the bottom center ring (Figure 8).

In TD3, the lone pairs of the hydroxyl oxygen atoms of Tyr124 and Tyr337 performed a pi-lone pair interaction with the ligand. Phe338, Phe297 and His447 showed pi-alkyl type interactions and Tyr341 showed a pi-pi stack type interaction with the upper central aromatic ring, and Trp286 performed a pi-pi T-shaped interaction with the lower central aromatic ring, according to Figure 9.

TD4 shows a hydrogen bond with Tyr337, in addition to the pi-pi T-shaped interactions performed with the aromatic rings. Tyr124 also performs a pi-pi T-shaped interaction with the same rings, in addition to a pi-lone pair between the residue oxygen and the aromatic heterocycle. Trp286 and Tyr341 perform pi-pi stack interactions, and Tyr341 also performs pi-pi T-shaped interactions with the ligand. Trp86 and Leu76 make pi-alkyl-type interactions (Figure 10).

All the compounds interact with Tyr337 and Tyr341, important residues concerning the steric effect of the ligand produced in the binding site. The highest scores presented for each compound are shown in Table I. Higher scores represent greater interaction affinity. All synthesized dimers obtained higher scorers than tacrine and the co-crystallized ligand 1YL (Dihydrotanshinone).

Table I. Molecular docking punctuation with Gold score function for the best poses.

Compound	Gold score Punctuation
Tacrine	58.64
1YL	50.76
TD1	68.36
TD2	72.01
TD3	71.94
TD4	74.39

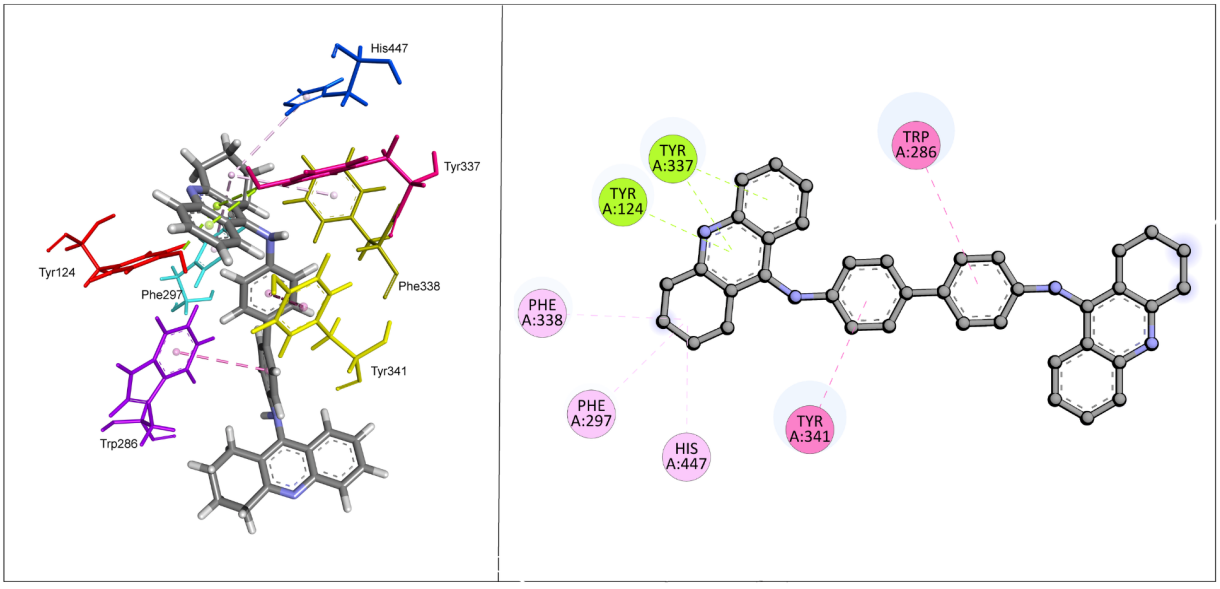

Figure 9. The 3D (left) and 2D (right) diagrams show the interactions of TD3 at the binding site of human acetylcholinesterase (PD ID 4M0E). The figure was generated by the Biovia Discovery Studio Visualizer software (v21.1.0.20298, BIOVIA, San Diego, CA, USA).

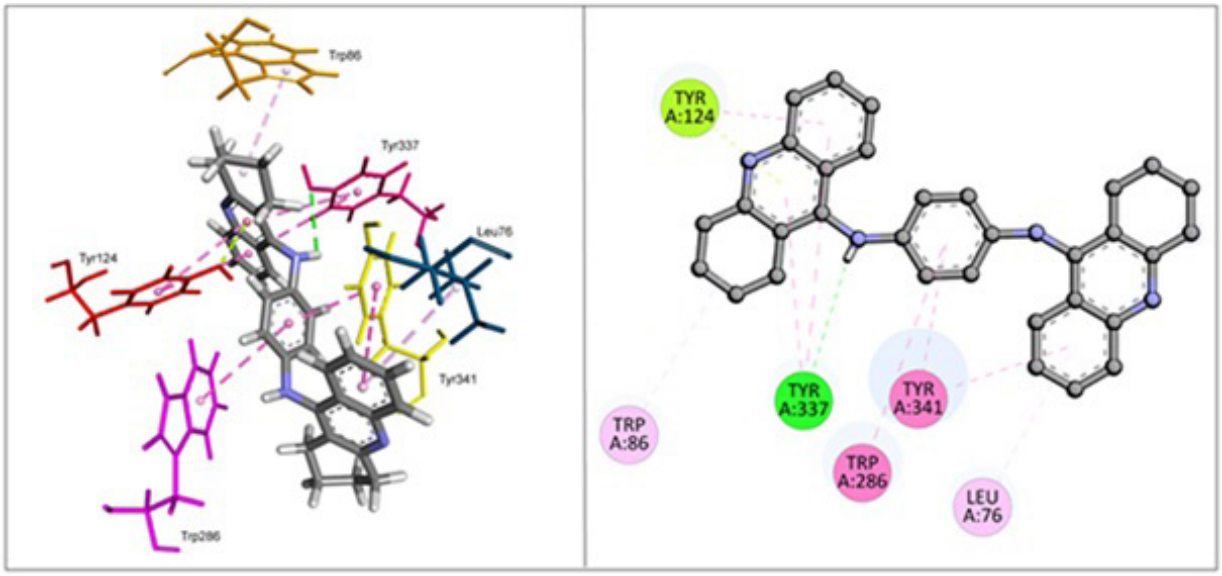

Figure 10. The 3D (left) and 2D (right) diagrams show the interactions of TD4 at the binding site of human acetylcholinesterase (PD ID 4M0E). The figure was generated by the Biovia Discovery Studio Visualizer software (v21.1.0.20298, BIOVIA, San Diego, CA, USA).

Quantum studies

HOMO and LUMO energy orbitals can be used for characterization in charger transfer complexes (Kumar et al. 2021). While HOMO energy measures the electron-donate capacity, LUMO energy measures the electron-acceptor character of a compound (Miar et al. 2021). It is possible to analyze the main collaborations of atomic orbitals, on the surfaces of the HOMO and LUMO molecular orbitals, according to Figure 11.

For tacrine, the main atomic orbitals that collaborate in HOMO are P_y of atom C3, P_z in N9, C15, and N1, and S on atom C4. LUMO shows P_x of atom C2, P_y on atom C3 P_z on C4 and C7, and S on C12 and C14 atoms as main collaborations.

TD1 presented the main collaborations with S on the C27 atom, Pz on the N25 and C39 atoms, and Py on the C26 atom in HOMO. However, in LUMO the main atomic orbitals are S on the C15, C37, C24, C43, C23, and C35 atoms and Px on the C13 atom. In TD2, the main atomic orbitals are Py on the C26 atom and S on the C27, C12, C18, C23, and C5 atoms for HOMO, and in LUMO S on the C15 and C4 atoms and Py on the C43, C13, C11, and C8. For TD3, Py on the C27 atom, Pz on the C12 atom, and S on the C42, C11, C15, C28, and C24 atoms are the principal atomic orbitals for HOMO, and S on the C15, C17, C16, C20, and C24 atoms, and Px on the C15, C17, C16, C20, and C24 atoms. atoms C13 and C26 for LUMO. TD4 presented S on atoms C36, C11, C21, and C7, Py on atom C12 and Pz on atoms C12 and C18 for HOMO, and S on atoms C18, C15, C17, C28 C16, and C29 and Px on atom C33 for LUMO as main collaborations.

TD1, TD2, TD3, and TD4 showed higher HOMO probability density in the centre of the structure, while LUMO probability density was predominantly present in the tacrine-derived parts. The energy values of HOMO, LUMO, and gap are presented in Table II.

Generally, as E_{HOMO}, which is correlated with ionization energy increases, so does the ability to donate electrons. In the same way, when E_{LUMO} decreases is related to electron affinity, and receiving electrons becomes easier (Honório & Da Silva 2003). All the dimers have a better

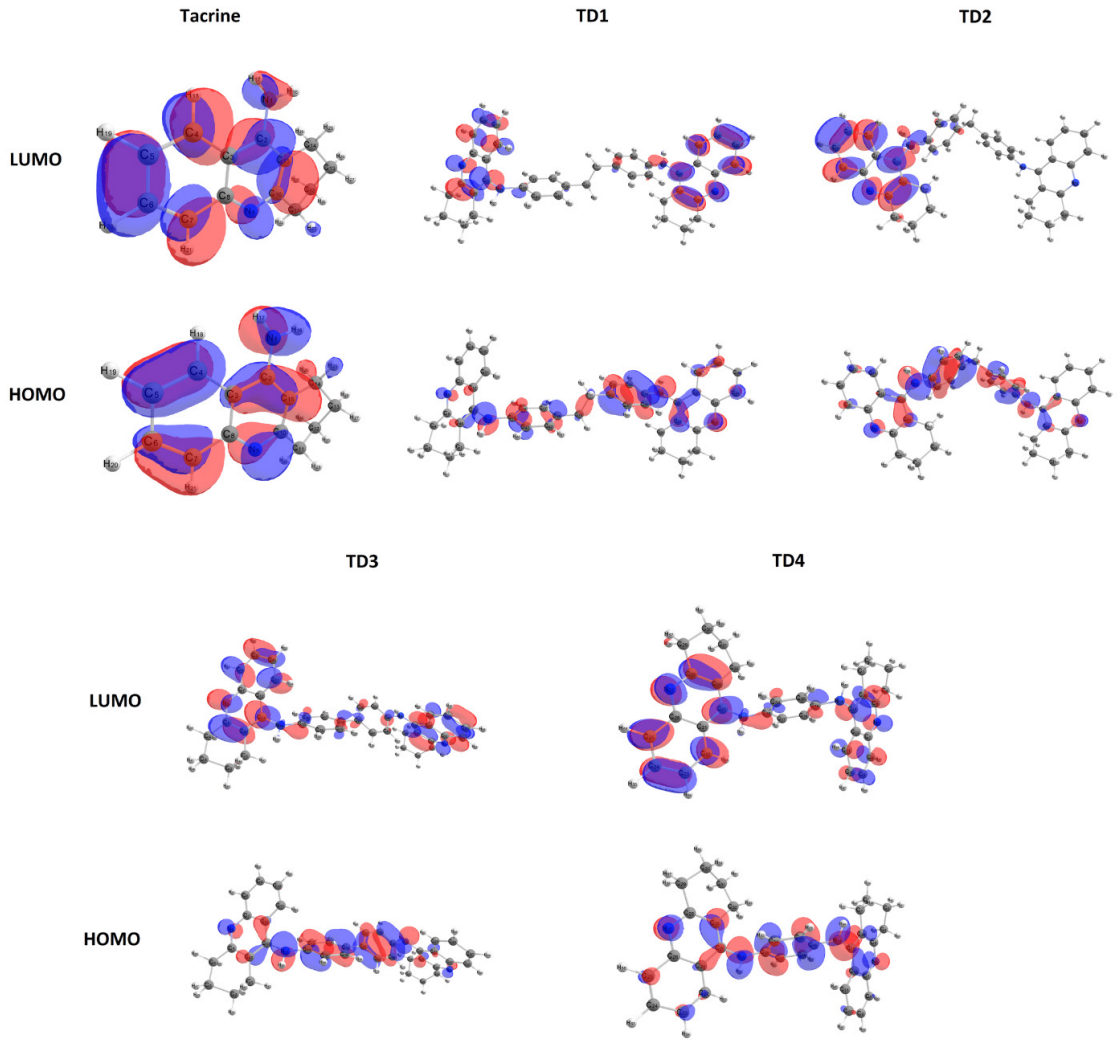

Figure 11. Surfaces of HOMO and LUMO to tacrine, TD1, TD2, TD3, and TD4 were obtained through the DFT method using the def2-TZVPP set of basic functions and B3LYP functional. In red are the positive phases and in blue are the negative phases of the orbitals.

Table II. HOMO, LUMO, and Gap (eV) energy values for the studied compounds.

Compound	HOMO (eV)	LUMO (eV)	Gap (eV)
Tacrine	-5.668	-1.150	4.518
TD1	-5.472	-1.483	3.989
TD2	-5.487	-1.552	3.935
TD3	-5.257	-1.506	3.751
TD4	-5.269	-1.525	3.744

electron donor and electron acceptor capacity than the tacrine standard. Furthermore, the gaps between the dimers are close, differing from tacrine by approximately 0.5 eV.

Quantum studies

The analysed compound, TD1, presents several advantageous ADMET properties that highlight its potential as a drug candidate. Despite its high molecular weight (574.77 g/mol) and lipophilicity (LogP 9.81), TD1 exhibits excellent intestinal absorption (91.73%), indicating efficient uptake in the gastrointestinal tract. Its role as a P-glycoprotein substrate and inhibitor

could be leveraged for targeted modulation of drug transport pathways, which may enhance bioavailability or therapeutic efficacy in specific contexts. Additionally, its low skin permeability (logKp = -2.73) reduces the likelihood of unintended systemic exposure through dermal routes, aligning with safety considerations.

In terms of metabolic behavior, TD1 shows a selective inhibition profile, targeting CYP1A2 while avoiding inhibition of key enzymes such as CYP2C19, CYP2C9, and CYP2D6, reducing the risk of widespread metabolic interactions. It is also a substrate for CYP2D6 and CYP3A4, two critical enzymes for drug metabolism, suggesting predictable metabolic pathways. Importantly, the compound avoids AMES toxicity and hERG I inhibition, indicating a reduced risk of genotoxicity and severe cardiotoxicity, respectively. Furthermore, its fraction unbound (0.34) supports adequate free drug availability for pharmacological activity, and the absence of renal OCT2 substrate activity minimizes the risk of nephrotoxicity.

Toxicological evaluations add to TD1's promising profile. The compound demonstrates acceptable safety margins in acute oral toxicity (LD50 = 3.06 mol/kg) and chronic toxicity (LOAEL = 0.91 log mg/kg_bw/day), along with no skin sensitization risk. It also exhibits manageable environmental toxicity, with low impact in ecological systems. These beneficial characteristics make TD1 an attractive scaffold for further optimization, focusing on refining solubility and lipophilicity to enhance its overall therapeutic potential while maintaining its favourable ADMET profile.

The compound TD4 showcases a promising pharmacokinetic and ADMET profile, supporting its potential as a therapeutic candidate. Despite its high lipophilicity (LogP 8.03) and substantial molecular weight (470.62 g/mol), TD4 demonstrates excellent intestinal absorption (92.63%) and robust Caco-2 permeability, indicating efficient absorption through the gastrointestinal tract. Additionally, its interaction with P-glycoprotein as both a substrate and inhibitor suggest potential modulation of efflux mechanisms, which may enhance its bioavailability and distribution. While its overall GI absorption is predicted to be low, targeted formulation strategies could help overcome this limitation.

Metabolically, TD4 is a substrate for the CYP2D6 and CYP3A4 enzymes, while selectively inhibiting CYP1A2 and CYP2C19, which minimizes the likelihood of broad-spectrum drug-drug interactions. The compound's safety profile is notable, being non-mutagenic (AMES negative) and lacking inhibition of hERG I channels, thus reducing the risk of genotoxicity and severe cardiotoxicity. Furthermore, its chronic toxicity (LOAEL = 1.309 log mg/kg_bw/day) and acute oral toxicity (LD50 = 2.458 mol/kg) fall within acceptable ranges, supporting its viability for further preclinical evaluations.

Distribution properties, such as moderate protein binding (fraction unbound = 0.28) and restricted blood-brain barrier permeability (log BB = -0.278), suggest TD4's potential as a peripheral agent with reduced CNS-related side effects. Its low skin permeability (log Kp = -2.73) and lack of skin sensitization risks further emphasize its favourable safety profile. Overall, TD4's strengths lie in its balanced pharmacokinetic characteristics, selective metabolic pathways, and manageable toxicity, making it an attractive lead for further optimization and drug development.

Comparing the profiles of TD4 and the previous compound, both demonstrate favourable pharmacokinetic and ADMET characteristics, with TD4 standing out for its higher intestinal absorption and selective metabolic interactions, while the first compound exhibits broader tissue distribution and slightly lower predicted toxicity,

highlighting their complementary potential for further therapeutic exploration.

CONCLUSIONS

The results obtained in this study provide relevant contributions regarding investigations into future drug design strategies or clinical implications in the treatment of AD. The current data obtained not only confirm the anticholinesterase activity of the compounds under study, also in vivo, but also demonstrate that they have a very promising neuroprotective effect, which is of fundamental importance as target molecules for the treatment of neurodegenerative disorders. Furthermore, the pharmacokinetic profiles of the compounds, particularly TD4 and the previously studied molecule, exhibit favorable characteristics, with TD4 showing higher intestinal absorption and selective metabolic interactions, while the first compound demonstrates broader tissue distribution and slightly lower predicted toxicity. However, further studies are needed to elucidate the mechanism of action involved in these responses. These findings corroborate data in the literature and pave the way for the development of new and promising hybrids of tacrine and/or MTDLs that may aid in the treatment of Alzheimer's disease.

Acknowledgments

This work was supported by the Conselho Nacional de Desenvolvimento Científico e Tecnológico (CNPq), Coordenação de Aperfeiçoamento de Pessoal de Ensino Superior (CAPES, Finance code 001), Fundação de Amparo à Pesquisa de Santa Catarina (FAPESC) and Fundação de Amparo à Pesquisa do Estado de Minas Gerais (FAPEMIG). S.S. and J.R. would also like to acknowledge CNPq (grant: 316687/2023-5, 309975/2022-0, 404172/2023-7, 405655/2023-1). S.S. would also like to acknowledge FAPEG (04/2023; EQU2023101000020). S.S. would also like to acknowledge FAPEG (04/2023; EQU2023101000020). Partial support was provided by the Spanish Ministry of Science, Innovation and Universities; Spanish Research Agency; and European Regional Development Funds (grant PID2021-122650OB-I00) to M.I.R.-F.

SUPPLEMENTARY MATERIAL

Figure S1.
Tables SI-SIII.

REFERENCES

AGUIRRE-RUEDA D, GUERRA-OJEDA S, ALDASORO M, IRADI A, OBRADOR E, ORTEGA A, MAURICIO MD, VILA JM & VALLES SL. 2015. Astrocytes protect neurons from Aβ1-42 peptide-induced neurotoxicity increasing TFAM and PGC-1 and decreasing PPAR-γ and SIRT-1. Int J Med Sci 12: 48.

AMOAH SK, DALLA VECCHIA MT, PEDRINI B, CARNHELUTTI GL, GONÇALVES EA, DOS SANTOS DA, BIAVATTI MW & DE SOUZA MM. 2015. Inhibitory effect of sesquiterpene lactones and the sesquiterpene alcohol aromadendrane-4β,10α-diol on memory impairment in a mouse model of Alzheimer. Eur J Pharmacol 769: 195-202.

AU J, BUSCHKUEHL M, DUNCAN GJ & JAEGGI SM. 2016. There is no convincing evidence that working memory training is NOT effective: A reply to Melby-Lervåg and Hulme (2015). Psychon Bull Rev 23: 331-337.

AZAMBUJA AS, CORREA L, GABIATTI BP, MARTINS GR, FRANCO ÁO, RIBEIRO MFM & BALDO G. 2018. Aversive and non-aversive memory impairment in the mucopolysaccharidosis II mouse model. Metab Brain Dis 33: 343-345.

BALDUCCI C & FORLONI G. 2014. In Vivo Application of beta Amyloid Oligomers. Curr Pharm Des 20: 2491-2505.

BARAL S, CHO DH, PARIYAR R, YOON CS, CHANG B, KIM DS, CHO HK, KIM SY, OH H & KIM YC. 2015. The Ameliorating Effect of Myrrh on Scopolamine-Induced Memory Impairments in Mice. Evid Based Complement Alternat Med 2015: 925432.

BARNHART CD, YANG D & LEIN PJ. 2015. Using the Morris Water Maze to Assess Spatial Learning and Memory in Weanling Mice. PloS one 10: e0124521.

BOTTESELLE GV ET AL. 2021. Catalytic antioxidant activity of bis-aniline-derived diselenides as GPx mimics. Molecules 26: 4446.

BRADFORD MM. 1976. A rapid and sensitive method for the quantitation of microgram quantities of protein utilizing the principle of protein-dye binding. Anal Biochem 72: 248-254.

BRADLEY-WHITMAN MA & LOVELL MA. 2015. Biomarkers of lipid peroxidation in Alzheimer disease (AD): an update. Arch Toxicol 89: 1035-1044.

BREIJYEH Z & KARAMAN R. 2020. Comprehensive review on Alzheimer's disease: Causes and treatment. Molecules 25: 5789.

BURKER GT ET AL. 2023. Selenylated Imidazo[1,2-a]pyridine Induces Cell Senescence and Oxidative Stress in Chronic Myeloid Leukemia Cells. Molecules 28: 893.

CAZARIN CA, DALMAGRO AP, GONÇALVES AE, BOEING E, DA SILVA LM, CORRÊA R, KLEIN-JÚNIOR LC, PINTO BC, LORENZETT TS & DA COSTA SOBRINHO TU. 2021. Usnic acid enantiomers restore cognitive deficits and neurochemical alterations induced by Aβ1-42 in mice. Behav Brain Res 397: 112945.

CHAAYA N, BATTLE AR & JOHNSON LR. 2018. An update on contextual fear memory mechanisms: Transition between Amygdala and Hippocampus. Neurosci Biobehav Rev 92: 43-54.

CHANG YT, CHANG WN, TSAI NW, HUANG CC, KUNG CT, SU YJ, LIN WC, CHENG BC, SU CM & CHIANG YF. 2014. The roles of biomarkers of oxidative stress and antioxidant in Alzheimer's disease: a systematic review. Biomed Res Int 82303.

CHARISIS S, NTANASI E, YANNAKOULIA M, ANASTASIOU CA, KOSMIDIS MH, DARDIOTIS E, HADJIGEORGIOU G, SAKKA P, VESKOUKIS AS & KOURETAS D. 2021. Plasma GSH levels and Alzheimer's disease. A prospective approach.: Results from the HELIAD study. Free Radic Biol Med 162: 274-282.

CHEN JH, KE KF, LU JH, QIU YH & PENG YP. 2015. Protection of TGF-β1 against Neuroinflammation and Neurodegeneration in Aβ1–42-Induced Alzheimer's Disease Model Rats. PloS one 10: e0116549.

CHEUNG P, GARY EN, SHIOMI K & ROSENBERRY TL. 2013. Structures of human acetylcholinesterase bound to dihydrotanshinone I and territrem B show peripheral site flexibility. ACS Med Chem Lett 4: 1091-1096.

CIOFFI F, ADAM RHI, BANSAL R & BROERSEN K. 2021. A review of oxidative stress products and related genes in early Alzheimer's disease. J Alzheimer's Dis 83: 977-1001.

CRYSTAL JD. 2016. Animal models of source memory. J Exp Anal Behav 105: 56-67.

CSIZMADIA P. 1999. in Proceedings of The 3rd International Electronic Conference on Synthetic Organic Chemistry, MDPI, Sciforum.net. p. 1775.

DE AQUINO RAN, MODOLO LV, ALVES RB & DE FÁTIMA A. 2013. Synthesis, kinetic studies and molecular modeling of novel tacrine dimers as cholinesterase inhibitors. Org Biomol Chem 11: 8395-8409.

DELGADO-PERAZA F, NOGUERAS-ORTIZ CJ, VOLPERT O, LIU D, GOETZL EJ, MATTSON MP, GREIG NH, EITAN E & KAPOGIANNIS E. 2021. Neuronal and Astrocytic Extracellular Vesicle Biomarkers in Blood Reflect Brain Pathology in Mouse Models of Alzheimer's Disease. Cells 10: 993.

DI L, KERNS EH, FAN K, MCCONNELL OJ & CARTER GT. 2003. High throughput artificial membrane permeability assay for blood–brain barrier. Eur J Med Chem 38: 223-232.

DOS SANTO DC ET AL 2021. Apoptosis oxidative damage-mediated and antiproliferative effect of selenylated imidazo[1,2-a]pyridines on hepatocellular carcinoma HepG2 cells and in vivo. J Biochem Mol Toxicol 35: e22663.

DOS SANTOS DC, RAFIQUE J, SABA S, FRINEVICIUS VMAS, FILHO DW, ZAMONER A, BRAGA AL, PEDROSA RC & OURIQUE F. 2022. IP-Se-06, a Selenylated Imidazo[1,2-a]pyridine, Modulates Intracellular Redox State and Causes Akt/mTOR/HIF-1α and MAPK Signaling Inhibition, Promoting Antiproliferative Effect and Apoptosis in Glioblastoma Cells. Oxid Med Cell Longev 3710449.

ESQUERDA-CANALS G, MONTOLIU-GAYA L, GÜELL-BOSCH J & VILLEGAS S. 2017. Mouse Models of Alzheimer's Disease. J Alzheimer's Dis 57: 1171-1183.

FANG Y, DOYLE MF, CHEN J, ALOSCO ML, MEZ J, SATIZABAL CL, QIU WQ, MURABITO JM & LUNETTA KL. 2022. Association between inflammatory biomarkers and cognitive aging. Plos one 17: e0274350.

FERMIANO MH ET AL. 2024. Selenium-Containing (Hetero) Aryl Hybrids as Potential Antileishmanial Drug Candidates: In Vitro Screening against L. amazonensis. Biomedicines 12: 213.

FOTUHI SN, KHALAJ-KONDORI M, FEIZI MAH & TALEBI M. 2020. Memory-related process in physiological status and alzheimer's disease. Mol Biol Rep 47: 4651-4657.

FRANCO MS, SABA S, RAFIQUE J & BRAGA AL. 2021. KIO4-mediated Selective Hydroxymethylation/Methylenation of Imidazo-Heteroarenes: A Greener Approach. Angew Chem Int Ed Engl 60: 18454-18460.

FRIZON TEA, CARARO JS, SABA S, DAL-PONT GC, MICHELS M, BRAGA HC, PIMENTEL T, DAL-PIZZOL F, VALVASSORI SS & RAFIQUE J. 2020. Synthesis of novel selenocyanates and evaluation of their effect in cultured mouse neurons submitted to oxidative stress. Oxid Med Cell Longev 5417024.

FU Q, GAO N, YU N, MA G, DU Y, WANG F, SU Q & CHE F. 2014. Diazoxide Pretreatment Prevents Aβ1–42 Induced Oxidative Stress in Cholinergic Neurons Via Alleviating NOX2 Expression. Neurochem Res 39: 1313-1321.

GASCHLER MM & STOCKWELL BR. 2017. Lipid peroxidation in cell death. Biochem Biophys Res Commun 482: 419-425.

GELLHAAR S, SUNNEMARK D, ERIKSSON H, OLSON L & GALTER D. 2017. Myeloperoxidase-immunoreactive cells are significantly increased in brain areas affected by neurodegeneration in Parkinson's and Alzheimer's disease. Cell Tissue Res 369: 445-454.

GONÇALVES AE, BÜRGER C, AMOAH SK, TOLARDO R, BIAVATTI MR & DE SOUZA MM. 2012. The antidepressant-like effect ofHedyosmum brasilienseand its sesquiterpenelactone, podoandin in mice: Evidence for the involvement of adrenergic, dopaminergic and serotonergic systems. Eur J Pharmacol 674: 307-314.

GONÇALVES AE, MALHEIROS Â, CASARIN CA, DE FRANÇA L, PALOMINO-SALCEDO DL, FERREIRA LL, ANDRICOPULO AD, DÁVILA-RODRÍGUEZ MJ, LACAVA LC & DE OLIVEIRA AS. 2021. 2',6'-dihydroxy-4'-methoxy Dihydrochalcone Improves the Cognitive Impairment of Alzheimer's Disease: A Structure-activity Relationship Study. Curr Top Med Chem 21: 1167-1185.

GREEN PS, MENDEZ AJ, JACOB JS, CROWLEY JR, GROWDON W, HYMAN BT & HEINECKE JW. 2004. Neuronal expression of myeloperoxidase is increased in Alzheimer's disease. J Neurochem 90: 724-733.

HAMULAKOVA S, KUDLICKOVA Z, JANOVEC L, MEZENCEV R, DECKNER ZJ, CHERNOFF YO, JANOCKOVA J, IHNATOVA V, BZONEK P & NOVAKOVA N. 2021. Design and synthesis of novel tacrine–indole hybrids as potential multitarget-directed ligands for the treatment of Alzheimer's disease. Future Med Chem 13: 785-804.

HANWELL MD, CURTIS DE, LONIE DC, VANDERMEERSCH T, ZUREK E & HUTCHISON GR. 2012. Avogadro: an advanced semantic chemical editor, visualization, and analysis platform. J Cheminf 4: 1-17.

HASSANZADEH G, HOSSEINI A, PASBAKHSH P, AKBARI M, GHAFFARPOUR M, TAKZARE N & ZAHMATKESH M. 2015. Trimetazidine prevents oxidative changes induced in a rat model of sporadic type of Alzheimer's disease. Acta Med Iran 53: 17-24.

HERRERA-AROZAMENA C, ESTRADA-VALENCIA M, PEREZ C, LAGARTERA L, MORALES-GARCIA JA, PEREZ-CASTILLO A, FRANCO-GONZALEZ JF, MICHALSKA P, DUARTE P & LEON R. 2020a. Tuning melatonin receptor subtype selectivity in oxadiazolone-based analogues: Discovery of QR2 ligands and NRF2 activators with neurogenic properties. Eur J Med Chem 190: 112090.

HERRERA-AROZAMENA C, ESTRADA-VALENCIA M, MARTÍ-MARÍ O, PÉREZ C, DE LA FUENTE REVENGA M, VILLALBA-GALEA C & RODRÍGUEZ-FRANCO MI. 2020b. Optical control of muscular nicotinic channels with azocuroniums, photoswitchable azobenzenes bearing two N-methyl-N-carbocyclic quaternary ammonium groups. Eur J Med Chem 200: 112403.

HERRERA-AROZAMENA C ET AL. 2022. Resveratrol-Based MTDLs to Stimulate Defensive and Regenerative Pathways and Block Early Events in Neurodegenerative Cascades. J Med Chem 65: 4727-4751.

HONÓRIO KM & DA SILVA ABF. 2003. An AM1 study on the electron-donating and electron-accepting character of biomolecules. Int J Quantum Chem 95: 126-132.

ISLAM TM. 2017. Oxidative stress and mitochondrial dysfunction-linked neurodegenerative disorders. Neurol Res 39: 73-82.

IZQUIERDO I, BARROS DM, MELLO E SOUZA T, DE SOUZA MM, IZQUIERDO MM & MEDINA JH, 1998. Mechanisms for memory types differ. Nature 393: 635-636.

IZQUIERDO I, FURINI CR & MYSKIW JC. 2016. Fear memory. Physiol Rev 96: 695-750.

IZQUIERDO I & MEDINA JH. 1997. Memory formation: the sequence of biochemical events in the hippocampus and its connection to activity in other brain structures. Neurobiol Learn Mem 68: 285-316.

JAFARI MR, ZARRINDAST MR & DJAHANGUIRI B. 2006. Influence of cholinergic system modulators on morphine state-dependent memory of passive avoidance in mice. Physiol Behav 88: 146-151.

JIANG L, HUANG M, XU S, WANG Y, AN P, FENG C, CHEN X, WEI X, HAN Y & WANG Q. 2016. Bis(propyl)-cognitin Prevents β-amyloid-induced Memory Deficits as Well as Synaptic Formation and Plasticity Impairments via the Activation of PI3-K Pathway. Mol Neurobiol 53: 3832-3841.

JIANG ZY, HUNT JV & WOLFF SP. 1992. Ferrous ion oxidation in the presence of xylenol orange for detection of lipid hydroperoxide in low density lipoprotein. Anal Biochem 202: 384-389.

JURRUS E ET AL. 2018. Improvements to the APBS biomolecular solvation software suite. Protein Sci 27: 112-128.

KAUSHIK V, SMITH ST, MIKOBI E & RAJI MS. 2018. Acetylcholinesterase Inhibitors: Beneficial Effects on Comorbidities in Patients With Alzheimer's Disease. Am J Alzheimers Dis Other Demen 33: 73-85.

KHAN S, BARVE KH & KUMAR MS. 2020. Recent advancements in pathogenesis, diagnostics and treatment of Alzheimer's disease. Curr Neuropharmacol 18: 1106-1125.

KUMAR A, BANERJEE K, ERVASTI MM, KEZILEBIEKE S, DVORAK M, RINKE P, HARJU A & LILJEROTH P. 2021. Electronic characterization of a charge-transfer complex monolayer on graphene. ACS Nano 15: 9945-9954.

LEE C, YANG W & PARR RG. 1988. Development of the Colle-Salvetti correlation-energy formula into a functional of the electron density. Phys Rev B 37: 785.

LOPEZ OL & KULLER LH. 2019. Chapter 9 - Epidemiology of aging and associated cognitive disorders: Prevalence and incidence of Alzheimer's disease and other dementias. Handb Clin Neurol 167: 139-148.

LUEPTOW LM. 2017. Novel Object Recognition Test for the Investigation of Learning and Memory in Mice. JoVE 2017: e55718.

MARKLUND S & MARKLUND G. 1974. Involvement of the superoxide anion radical in the autoxidation of pyrogallol and a convenient assay for superoxide dismutase. Eur J Biochem 47: 469-474.

MARTÍN-SÁNCHEZ A, PIÑERO J, NONELL J, ARNAL J, RIBE EM, NEVADO-HOLGADO A, LOVESTONE S, SANZ F, FURLONG LI & VALVERDE O. 2021. Comorbidity between Alzheimer's disease and major depression: a behavioural and transcriptomic characterization study in mice. Alzheimers Res Ther 13: 1-19.

MARUCCI G, BUCCIONI M, DAL BEN D, LAMBERTUCCI C, VOLPINI R & AMENTA F. 2021. Efficacy of acetylcholinesterase inhibitors in Alzheimer's disease. Neuropharmacology 190: 108352.

MIAR M, SHIROUDI A, POURSHAMSIAN K, OLIAEY AR & HATAMJAFARI F. 2021. Theoretical investigations on the HOMO–LUMO gap and global reactivity descriptor studies, natural bond orbital, and nucleus-independent chemical shifts analyses of 3-phenylbenzo[d]thiazole-2(3H)-imine and its para-substituted derivatives: Solvent and substituent effects. J Chem Res 45: 147-158.

MISHRA N, SASMAL D & SINGH KK. 2013. Attenuating Aβ1–42-induced toxicity by a novel acetylcholinesterase inhibitor. Neurosci 250: 309-319.

MOHAMED T, SHAKERI A & RAO PP. 2016. Amyloid cascade in Alzheimer's disease: Recent advances in medicinal chemistry. Eur J Med Chem 113: 258-272.

MORAES CAO ET AL. 2023. Urea Hydrogen Peroxide and Ethyl Lactate, an Eco-Friendly Combo System in the Direct C(sp2)–H Bond Selenylation of Imidazo[2,1-b]thiazole and Related Structures. ACS Omega 8: 39535-39545.

MORRIS RG, GARRUD P, AL RAWLINS J & O'KEEFE J. 1982. Place navigation impaired in rats with hippocampal lesions. Nature 297: 681-683.

MOSS DE & PEREZ RG. 2021. Anti-Neurodegenerative Benefits of Acetylcholinesterase Inhibitors in Alzheimer's Disease: Nexus of Cholinergic and Nerve Growth Factor Dysfunction. Curr Alzheimer Res 18: 1010.

MOTA SI, COSTA RO, FERREIRA IL, SANTANA I, CALDEIRA GL, PADOVANO C, FONSECA AC, BALDEIRAS I, CUNHA C & LETRA L. 2015. Oxidative stress involving changes in Nrf2 and ER stress in early stages of Alzheimer's disease. Biochim Biophys Acta 1852: 1428-1441.

NAKAI T, YAMADA K & MIZOGUCHI H. 2021. Alzheimer's Disease Animal Models: Elucidation of Biomarkers and Therapeutic Approaches for Cognitive Impairment. Int J Mol Sci 22: 5549.

NEESE F. 2012. The ORCA program system. Wiley Interdiscip Rev Comput Mol Sci 2: 73-78.

NEPOVIMOVA E ET AL. 2021. Tacrine – Benzothiazoles: Novel class of potential multitarget anti-Alzheimeŕs drugs dealing with cholinergic, amyloid and mitochondrial systems. Bioorg Chem 107: 104596.

PARIZKOVA M, LERCH O, MOFFAT SD, ANDEL R, MAZANCOVA AF, NEDELSKA Z, VYHNALEK M, HORT J & LACZÓ J. 2018. The effect of Alzheimer's disease on spatial navigation strategies. Neurobiol Aging 64: 107-115.

PEDROSO GJ ET AL. 2023. Selenylated indoles: Synthesis, effects on lipid membrane properties and DNA cleavage. New J Chem 47: 2719-2726.

PENTKOWSKI NS, ROGGE-OBANDO KK, DONALDSON TN, BOUQUIN SN & CLARK BJ. 2021. Anxiety and Alzheimer's disease: Behavioral analysis and neural basis in rodent models of Alzheimer's-related neuropathology. Neurosci Biobehav Rev 127: 647-658.

PERATHONER S, CORDERO-MALDONADO ML & CRAWFORD AD. 2016. Potential of zebrafish as a model for exploring the role of the amygdala in emotional memory and motivational behavior. J Neurosci Res 94: 445-462.

PERSICHILLI S, GERVASONI J, DI NAPOLI A, FUSO A, NICOLIA V, GIARDINA B, SCARPA S, DESIDERIO C & CAVALLARO RA. 2015. Plasma thiols levels in Alzheimer's disease mice under diet-induced hyperhomocysteinemia: effect of S-adenosylmethionine and superoxide-dismutase supplementation. J Alzheimers Dis 44: 1323-1331.

PLUTA R, OUYANG L, JANUSZEWSKI S, LI Y & CZUCZWAR SJ. 2021. Participation of Amyloid and Tau Protein in Post-Ischemic Neurodegeneration of the Hippocampus of a Nature Identical to Alzheimer's Disease. Int J Mol Sci 22: 2460.

PREDIGER RD, FRANCO JL, PANDOLFO P, MEDEIROS R, DUARTE FS, DI GIUNTA G, FIGUEIREDO CP, FARINA M, CALIXTO JB &

TAKAHASHI RN. 2007. Differential susceptibility following β-amyloid peptide-(1–40) administration in C57BL/6 and Swiss albino mice: Evidence for a dissociation between cognitive deficits and the glutathione system response. Behav Brain Res 177: 205-213.

QIAN S, HE L, MAK M, HAN Y, HO CY & ZUO Z. 2014. Synthesis, biological activity, and biopharmaceutical characterization of tacrine dimers as acetylcholinesterase inhibitors. Int J Pharm 477: 442-453.

RAFIQUE J ET AL. 2020. Selenylated-oxadiazoles as promising DNA intercalators: Synthesis, electronic structure, DNA interaction and cleavage. Dyes Pigm 180: 108519.

RAY RS & KATYAL A. 2016 Myeloperoxidase: Bridging the gap in neurodegeneration. Neurosci Biobehav Rev 68: 611-620.

RAZA A, XIE W, KIM KH, DRONAMRAJU VR, WILLIAMS J, VINCE R & MORE SS. 2022. Dipeptide of ψ-GSH Inhibits Oxidative Stress and Neuroinflammation in an Alzheimer's Disease Mouse Model. Antioxidants 11: 1075.

ROLDAN-PENA JM ET AL. 2017. New tacrine dimers with antioxidant linkers as dual drugs: Anti-Alzheimer's and antiproliferative agents. Eur J Med Chem 138: 761-773.

SCHEIDE MR ET AL. 2020. Borophosphate glass as an active media for CuO nanoparticle growth: An efficient catalyst for selenylation of oxadiazoles and application in redox reactions. Sci Rep 10: 15233.

SCHELTENS P, BLENNOW K, BRETELER MM, DE STROOPER B, FRISONI GB, SALLOWAY S & DER FLIER WMV. 2016. Alzheimer's disease. Lancet 388: 505-517.

SEDLAK J & LINDSAY RH. 1968. Estimation of total, protein-bound, and nonprotein sulfhydryl groups in tissue with Ellman's reagent. Anal Biochem 25: 192-205.

SHARMA A & GOYAL R. 2020. Long-term exposure to constant light induces dementia, oxidative stress and promotes aggregation of sub-pathological Aβ42 in Wistar rats. Pharmacol Biochem Behav 192: 172892.

SHEN L, YAN M & HE L. 2016. D5 receptor agonist 027075 promotes cognitive function recovery and neurogenesis in a Aβ1-42-induced mouse model. Neuropharmacology 105: 72-83.

SHRESTHA P & KLANN E. 2016. Lost memories found. Nature 531: 450-451.

SIMONI E ET AL. 2017. Multitarget drug design strategy in Alzheimer's disease: Focus on cholinergic transmission and amyloid-β aggregation. Future Med Chem 9: 953-963.

SÖLLVANDER S, NIKITIDOU E, BROLIN R, SÖDERBERG L, SEHLIN D, LANNFELT L & ERLANDSSON A. 2016. Accumulation of amyloid-β by astrocytes result in enlarged endosomes and microvesicle-induced apoptosis of neurons. Mo. Neurodegener 11: 1-19.

SPILOVSKA K, KORABECNY J, NEPOVIMOVA E, DOLEZAL R, MEZEIOVA E, SOUKUP O & KUCA K. 2017. Multitarget Tacrine Hybrids with Neuroprotective Properties to Confront Alzheimer's Disease. Curr Top Med Chem 17: 1006-1026.

TERRANOVA JI, YOKOSE J, OSANAI H, MARKS WD, YAMAMOTO J, OGAWA SK & KITAMURA T. 2022. Hippocampal-amygdala memory circuits govern experience-dependent observational fear. Neuron 110: 1416-1431. e13.

TIAN H, DING N, GUO M, WANG S, WANG Z, LIU H, YANG J, LI Y, REN J & JIANG J. 2019. Analysis of Learning and Memory Ability in an Alzheimer's Disease Mouse Model using the Morris Water Maze. JoVE 2019: e60055.

VALENCIA ME, HERRERA-AROZAMENA C, DE ANDRÉS L, PÉREZ C, MORALES-GARCÍA JA, PÉREZ-CASTILLO A, RAMOS E, ROMERO A, VIÑA D & YÁÑEZ M. 2018. Neurogenic and neuroprotective donepezil-flavonoid hybrids with sigma-1 affinity and inhibition of key enzymes in Alzheimer's disease. Eur J Med Chem 156:534-553.

VELOSO IC ET AL. 2021. A selanylimidazopyridine (3-SePh-IP) reverses the prodepressant-and anxiogenic-like effects of a high-fat/high-fructose diet in mice. J Pharm Pharmacol 73: 673-681.

VERDONK ML, CHESSARI G, COLE JC, HARTSHORN MJ, MURRAY CW, NISSINK JWM, TAYLOR RD & TAYLOR R. 2005. Modeling water molecules in protein-ligand docking using GOLD. J Med Chem 48: 6504-6515.

WALY OM, SAAD KM, EL-SUBBAGH HI, BAYOMI SM & GHALY MA. 2022. Synthesis, biological evaluation, and molecular modeling simulations of new heterocyclic hybrids as multi-targeted anti-Alzheimer's agents. Eur J Med Chem 231, 114152.

WEIGEND F & AHLRICHS R. 2005. Balanced basis sets of split valence, triple zeta valence and quadruple zeta valence quality for H to Rn: Design and assessment of accuracy. Phys Chem Chem Phys 7: 3297-3305.

WU WY, DAI YC, LI NG, DONG ZX, GU T, SHI ZH, XUE X, TANG XP & DUAN JA. 2017. Novel multitarget-directed tacrine derivatives as potential candidates for the treatment of Alzheimer's disease. J Enzyme Inhib Med Chem 32: 572-587.

YU L, WANG S, CHEN S, YANG H, LI X, XU Y & ZHU X. 2015. Orientin alleviates cognitive deficits and oxidative stress

in Aβ1-42-induced mouse model of Alzheimer's disease. Life Sci 121: 104-109.

ZHANG P ET AL. 2021. Design and synthesis of novel tacrine-dipicolylamine dimers that are multiple-target-directed ligands with potential to treat Alzheimer's disease. Bioorg Chem 116: 105387.

ZHANG YY, YANG LQ & GUO LM. 2015. Effect of phosphatidylserine on memory in patients and rats with Alzheimer's diseas. Genet Mol Res 14: 9325-9333.

ZHURKO GA & ZHURKO DA. 2005. Chemcraft: Academic version.

How to cite

GONÇALVES AE ET AL. 2025. New Tacrine Dimers Alleviate the Intracellular Amyloid-β-induced Cognitive Disturbance and Oxidative Stress in Mice. An Acad Bras Cienc 97: e20241163. DOI 10.1590/0001-3765202520241163.

ANA ELISA GONÇALVES[1]
https://orcid.org/0000-0002-5148-7184

OTTO SPIGARIOL[1]
https://orcid.org/0009-0008-5638-4716

LUÍSA M. DA SILVA[1,2]
https://orcid.org/0000-0001-5329-7301

YURI F. REGO[3]
https://orcid.org/0000-0003-4660-6852

CLARA HERRERA-AROZAMENA[4]
https://orcid.org/0000-0002-5894-128X

MARÍA ISABEL RODRÍGUEZ-FRANCO[4]
https://orcid.org/0000-0002-6500-792X

ÂNGELO DE FÁTIMA[3]
https://orcid.org/0000-0003-2344-5590

THIAGO HENRIQUE DORING[5]
https://orcid.org/0000-0002-3611-9105

LUCAS AUGUSTO ARAUJO[6]
https://orcid.org/0009-0001-7902-6136

MARIA LÍGIA R. MACEDO[6]
https://orcid.org/0000-0001-6969-6307

SUMBAL SABA[6]
https://orcid.org/0000-0002-6134-7249

JAMAL RAFIQUE[6,7]
https://orcid.org/0000-0002-2336-040X

ALDO S. DE OLIVEIRA[5]
https://orcid.org/0000-0001-7760-4484

MÁRCIA MARIA DE SOUZA[1]
https://orcid.org/0000-0002-6297-9635

[1]Universidade do Vale do Itajaí (UNIVALI), Programa de Pós-Graduação em Ciências Farmacêuticas, Rua Uruguai, 468, 88301-320 Itajaí, SC, Brazil

[2]Universidade Federal de Santa Catarina (UFSC), Laboratório de Farmacologia do Trato Gastrointestinal e suas Interações, Programa de Pós-graduação em Farmacologia, Campus Universitário, s/n, Sala 208, Bloco E, Prédio Administrativo, Córrego Grande, Trindade, 88040-900 Florianópolis, SC, Brazil

[3]Universidade Federal de Minas Gerais (UFMG), GEQOB, Departamento de Química, ICEx, Av. Pres. Antônio Carlos, 6627, Pampulha, 31270-901 Belo Horizonte, MG, Brazil

[4]Instituto de Química Médica, Consejo Superior de Investigaciones Científicas (IQM-CSIC), C/ Juan de la Cierva 3, E-28006 Madrid, Spain

[5]Universidade Federal de Santa Catarina (UFSC), Departamento de Ciências Exatas e Educação, Rua João Pessoa, 2750, Bairro Velha, 89036-002 Blumenau, SC, Brazil

[6]Universidade Federal de Goiás (UFG), LabSO, Instituto de Química (IQ), Av. Esperança, s/n, Campus Samambaia, 74690-900 Goiânia, GO, Brazil

[7]Universidade Federal do Mato Grosso do Sul (UFMS), Centro de Pesquisa e Inovação em Bioprospecção e Síntese de Produtos para a Saúde Humana e Animal (CIBSint), Instituto de Química (INQUI), Av. Costa e Silva, s/n, 79074-460 Campo Grande, MS, Brazil

Correspondence to: **Sumbal Saba, Jamal Rafique, Aldo S. de Oliveira, Márcia Maria de Souza**
E-mail: sumbalsaba@ufg.br, jamal.rafique@ufms.br, aldo.sena@ufsc.br, msouza@univali.br

Author contributions

Ana Elisa Gonçalves: Data curation, Investigation, Roles/Writing – original draft, Writing – review and editing. Otto Spigariol: Data curation, Investigation, Roles/Writing – original draft, Writing – review and editing. Luisa M. da Silva: Conceptualization, Formal analysis, Funding acquisition, Resources, Roles/Writing – original draft, Writing – review and editing. Yuri F. Rego: Synthesis of compounds, Writing – review and editing. Clara Herrera-Arozamena: PAMPA-BBB Data curation. María Isabel Rodríguez-Franco: PAMPA-BBB Assays, Funding acquisition, Resources, Writing and review. Ângelo de Fátima: Conceptualization, Funding acquisition, Resources, Writing – review and editing. Thiago Henrique Doring: Formal Analysis, Investigation, Writing – original draft. Lucas Augusto Araujo: Formal Analysis. Maria Lígia R. Macedo: Formal Analysis. Sumbal Saba: Funding acquisition, Resources, Investigation, Writing – review and editing. Jamal Rafique: Funding acquisition,

Resources, Formal analysis, Investigation, Writing – review and editing. Aldo S. de Oliveira: Methodology, Writing – review and editing. Márcia Maria de Souza: Conceptualization, Formal analysis, Funding acquisition, Resources, Supervision, Roles/ Writing – original draft, Writing – review and editing.